Anti-ESBL investigation of chitosan/silver nanocomposites against carbapenem resistant Pseudomonas aeruginosa

Article *in* International Journal of Biological Macromolecules · April 2019

DOI: 10.1016/j.ijbiomac.2019.03.238

CITATIONS
0

READS
176

5 authors, including:

Muthuchamy Maruthupandy
University of Chile
39 PUBLICATIONS **380** CITATIONS

SEE PROFILE

Wen-Jun Li
Sun Yat-Sen University
871 PUBLICATIONS **11,222** CITATIONS

SEE PROFILE

International Journal of Biological Macromolecules 132 (2019) 1221–1234

Contents lists available at ScienceDirect

International Journal of Biological Macromolecules

journal homepage: http://www.elsevier.com/locate/ijbiomac

Anti-ESBL investigation of chitosan/silver nanocomposites against carbapenem resistant *Pseudomonas aeruginosa*

Govindan Rajivgandhi [a,c], Muthuchamy Maruthupandy [b,*], Thangasamy Veeramani [c], Franck Quero [b], Wen-Jun Li [a]

[a] State Key Laboratory of Biocontrol and Guangdong Provincial Key Laboratory of Plant Resources, School of Life Sciences, Sun Yat-sen University, Guangzhou 510275, PR China
[b] Laboratorio de Nanocelulosa y Biomateriales, Departamento de Ingeniería Química, Biotecnología y Materiales, Facultad de Ciencias Físicas y Matemáticas, Universidad de Chile, Avenida Beauchef 851, Santiago, Chile
[c] Medical Microbiology & Marine Pharmacology Laboratory, Department of Marine Science, Bharathidasan University, Tiruchirappalli 620 024, Tamil Nadu, India

ARTICLE INFO

Article history:
Received 8 January 2019
Received in revised form 20 March 2019
Accepted 31 March 2019
Available online 01 April 2019

Keywords:
Chitosan/silver nanocomposites
Anti-ESBL activity
Toxicity effect

ABSTRACT

In the present investigation functional chitosan/silver nanocomposites (CS/Ag NCs) were successfully synthesized and found to possess favorable antibacterial activity against extended spectrum beta-lactasame (ESBL) producing *Pseudomonas aeruginosa*. Powder X-ray diffraction showed that the obtained CS/Ag NCs are constituted of highly crystalline Ag nanoparticles (NPs) embedded in an amorphous CS matrix material. Transmission electron microscopy (TEM) analysis provided structural information about CS/Ag NCs, revealing the formation of spherical cluster structures constituted of Ag NPs with size ranging from 6 to 18 nm embedded in the amorphous CS matrix. The minimum inhibitory concentration (MIC) and minimum bactericidal concentration (MBC) of Ag NPs and CS/Ag NCs were found to inhibit the ESBL producing *P. aeruginosa* at 80 μg/mL (76%) and 50 μg/mL (92%), respectively. Confocal laser scanning microscope (CLSM) and scanning electron microscopy (SEM) images revealed that *P. aeruginosa* experienced reduced cell viability and morphological cell membrane damage at desired MIC. The in-vivo toxicity effect of Ag NPs and CS/Ag NCs suggested an increased mortality rate when *Artemia franciscana* were exposed for 24 h to increasing concentrations of Ag NPs and CS/Ag NCs. Anti-ESBL activity and toxicity effect of CS/Ag NCs revealed that these NCs possess promising antibacterial properties to overcome numerous communicable bacterial strains.

1. Introduction

The antibiotic resistance is due to the enhanced evolutionary ability of microorganisms including bacteria, virus, fungi and parasites to fight and neutralize antibiotics [1]. Inabilities of antibiotics to kill infectious pathogens are the most condemnatory challenge to modern medicine and health care settings [2]. For instance, >40% of the urinary tract infection (UTI) pathogens seem to be heightening and become a rising therapeutic challenge for clinicians, particularly Gram-negative bacteria (GNB), which increase their antibiotic resistance nature. This has been reported to be one of the greatest challenges to public health [3]. According to the World Health Organization (WHO), the extensive uses of antibiotics, that are sometimes non-prescribed, have led to an expansion of bacterial antibiotic resistance [4]. The WHO outcome with respect to antimicrobial resistance (AMR) surveillance 2014 revealed that antibiotic resistance is serious and an emerging threat in treating bacterial infections [5]. Antibiotic resistant bacteria communicate with each other both by quorum sensing and inside the cell at the transcriptome level. It obliviously causes many types of asymptomatic infections leading to the development of multi drug resistance (MDR) bacteria [6]. In February 2017, the WHO announced first-ever list of twelve MDR bacteria that needed novel antimicrobial agents. These developed more resistance against almost all the current antibiotics. Among the twelve, seven bacteria were reported to possess resistance against β-lactam antibiotics and categorized as very "critical" [7]. β-lactam antibiotics have the ability to block bacterial cell wall very effectively. As a result, a drug has been developed against any types of bacterial infections for clinical treatment [8]. In recent years, some bacteria have developed resistance against β-lactam antibiotics such as penicillin and cephalosporin due to the production of β-lactamase [9]. β-lactamase is an enzyme produced by bacteria, which they use to hydrolyze β-lactam antibiotics. These bacteria contain β-lactamase coding gene, thereby inactivating the antibiotics and preventing cell lysis [10].

Among the GNB, *P. aeruginosa* is the second most common Gram-negative extended spectrum beta-lactamase(ESBL) producing bacteria causing UTI in hospitalized patients [11]. The WHO listed carbapenem-resistant *P. aeruginosa* as a top most critical pathogen, which desperately requires new treatment options [12]. In the US, 13–19% of MDR *P. aeruginosa* has been reported in health care related

* Corresponding author.
E-mail address: mmaruthupandy@yahoo.in (M. Maruthupandy).

https://doi.org/10.1016/j.ijbiomac.2019.03.238
0141-8130/

hospitalized patients yearly [13]. The MDR *P. aeruginosa* infections are associated with poor outcomes, including increased resource utilization, costs, morbidity, and mortality in hospital settings [14]. The patient-to-patient transmission of resistance strain is a prime factor for increasing of MDR *P. aeruginosa*, as well as newly acquired resistance owing to previous antibiotic usage [15].

Metal nanoparticles (gold and silver) show very good biological properties that are highly relevant for attention anti-bacterial, anti-fungal, anti-malarial and anti-cancer applications [16–18]. Among them, silver nanoparticles (Ag NPs) have shown excellent anti-bacterial activity of altered ESBL producing bacterial pathogens including *P. mirabilis* BDUMS 1 (KY617768), *E. coli* BDUMS 3 (KY617770), *P. aeruginosa* BDUMS 4, *P. aeruginosa* BDU 5, *K. pnumoniae* BDU 6 and *Enterobacter* sp. BDU 7 [19,20]. Furthermore, the antibacterial activity of Ag NPs relies on their morphology, size and size-distribution. Consequently, adjusting the size distribution of Ag NPs is challenging. Hence, progress on the improvement of the Ag NPs size distribution and dimensional stability have been reported by embedding Ag NPs in a polymer matrix [21,22].

Chitosan (CS) is a natural polysaccharide, mainly derived from the shell of marine crustaceans. CS possesses multifunctional properties including biodegradability, biocompatibility and antibacterial activity. It has been used as a matrix material to construct novel composite materials, while maintaining its efficient activities useful in numerous areas and particularly biomedical applications [23,24]. CS has been successfully used as a matrix material to form CS/Ag nanocomposites (NCs). CS was found to improve Ag NPs size-distribution as well stabilization but also promote additional antimicrobial properties to the resulting NCs [25–27]. Thus, combining CS and Ag NPs is very appropriate for multiple goals such as for biomedical, textile and food packaging applications [28,29].

A simple and significant biological path to produce the CS/Ag NCs is by using acetic acid as a reducing agent and CS as stabilizing agent. In the present work, the synthesized Ag NPs and CS/Ag NCs were characterized by UV–Visible (UV–Vis) spectrophotometry, Fourier-transform infrared (FTIR) spectroscopy, powder X-ray diffraction (XRD), thermagravimetric analysis (TGA) and morphologically by transmission electron microscopy (TEM) analysis. The antibacterial activity of synthesized Ag NPs and CS/Ag NCs was assessed against ESBL producing *P. aeruginosa* by minimum inhibitory concentration (MIC) and minimum bactericidal concentration (MBC) and their in-vivo toxicity was evaluated against *Artemia fanciscana*.

2. Materials and methods

2.1. Chemicals and glasswares

Acetic acid and chitosan powder with a molecular weight within the range of 310,000–375,000 Da, a viscosity range of 800–2000 cP and a deacetylation degree >75% were purchased from Aladdin Industrial Corporation and from Richjoint Chemicals (China), respectively. The molecular structure of chitosan is reported in Scheme 1. Analytical grade silver nitrate ($AgNO_3$) as well as glucose were obtained from Sinopharm chemicals (China) and were used as received, without further purification. All the glassware used in the present study was thoroughly washed with deionized water prior to use. All the media and chemicals were purchased from Hi-media laboratory (Mumbai, India) to perform biological characterization.

2.2. Synthesis of Ag NPs and CS/Ag NCs

The synthesis of CS/Ag NCs was carried out by stirring 100 mL of 0.7% (w/v) CS in 0.1 M glacial acetic acid until reaching pH 2.6. The viscous solution was stirred continuously overnight for complete dissolution of CS. Silver nitrate having a concentration of 0.05 M was subsequently used for the synthesis. A volume of ~40 mL of $AgNO_3$ solution was added

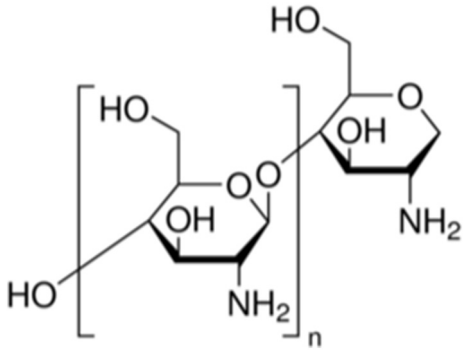

Scheme 1. Structure of high molecular weight chitosan.

to the viscous solution of chitosan and the mixture was stirred. The colorless solution was heated at 90 °C for 6 h to obtain an orange yellow CS/Ag NCs colloid. This color change was indicative of the formation of CS/Ag NCs, which was evidenced due to a color change from colorless to orange yellow color and monitored by UV–vis spectroscopy (Model: Shimadzu, UV-1750). After reaching room temperature, the orange-yellow solution was centrifuged at 9000 rpm for 30 min for eliminating undesired biggest CS/Ag NCs. The supernatant constitutes the CS/Ag NCs stock solution. Before further use, ~10 mL of stock solution was diluted in 90 mL of distilled water [30]. Ag NPs were prepared under the same condition, without CS.

2.2.1. Characterization of Ag NPs and CS/Ag NCs

The synthesized Ag and CS/Ag NCs were characterized by UV–Vis spectrophometry. The spectra were recorded using a Shimadzu UV-2450 spectrophotometer. FTIR spectra were recorded using a Nicolet FTIR (NEXUS-) spectrometer in the wavenumber range of 4000–400 cm^{-1}. TGA curves of Ag NPs and CS/Ag NCs were recorded using TGA-7 Perkin-Elmer under air atmosphere at a heating rate of 20 °C/min from 30 °C up to 800 °C. DTGA curves were obtained from the first derivative of the TGA curves. Powder XRD measurements were conducted using an advanced Rigaku D/max-RA X-ray diffractometer, equipped with CuKα radiation (λ = 1.54178 Å). The morphology and size of the Ag NPs and CS/Ag NCs were examined by TEM (Hitachi JEM-2100).

2.3. Collection and maintenance

Ten strains of Gram-negative uropathogens *P. aeruginosa*, which cause UTIs were obtained from the Department of Microbiology, K.A.P.V. Government Medical College, Tiruchirappalli, Tamil Nadu, India. The morphology and biochemical characterization of the selected strains were confirmed in our previous study [2]. After confirmation, the identified strains were streaked on nutrient agar slant and maintained at 4 °C until further use.

2.4. Detection of MDR strains of P. aeruginosa

All the ten *P. aeruginosa* strains were detected for their MDRs effect using specific UTI panel of Psudo 1 UTI 1- HX012, Psudo 2 UTI 2 - HX053, Pseudo 3 UTI 3- HX103 and Psudo 4 UTI 4- HX033 including imipenom (IPM-10 μg), aztreonam (AT-30 μg), cefoperazone/sulbactum (CFS-75/10 μg), piperacillin/tazobactam (PIT-100/10 μg), ceftazidime (CAZ-30 μg), netillin (NET-30 μg), cefotaxime (CAZ-30 μg), ciprofloxacin (CIP-5 μg), co-trimoxazole (COT-25 μg), gentamycin (GEN-10 μg), imipenem (IPM-10 μg), ticarcillin/clavulanic acid (TCC 75/10 μg), ciprofloxacin (CIP-5 μg), imipenem (IPM-10 μg), meropenem (MRP-10 μg), ertapenem (ETP-10 μg), cefoperazone/sulbactum (CFS-75/30 μg) piperacillin/tazobactam (PIT-100/10 μg) and nalidixic acid (NA-30 μg), nitrofurantoin (NT-300 μg), cephalothin (CEP-30 μg),

ampicillin (AMP-25 μg), co-Trimoxazole (Cot-25 μg), norfloxacin (NX 10 μg) by Kirby-Bauer disc diffusion method (CLSI Guidelines), following our previous study [4].

2.5. Screening of ESBLs producers

The ESBL producing ability of the 10 selected *P. aeruginosa* strains were phenotypically identified by agar disc diffusion method using Hexa G-minus 24 and HX096 disc method (CLSI, Guidelines, 2016) using cefpodoxime (CPD–10 μg), cefpodoxime/clavulanic acid (CCL–10/5 μg), ceftazidime (CAZ–30 μg), ceftazidime/clavulanic acid (CAC – 30/10 μg), cefotaxime (CTX – 30 μg), cefotaxime/clavulanic acid (CEC – 30/10 μg) [6]. In addition, the ESBL production was further confirmed by *E*-test MIC strip detection method. The two ends of the MIC gradient concentration discs were used. One end of each strip was impregnated with ceftazidime (0.50–32 μg/mL), cefotaxime (0.25–16 μg/mL). The other ends of the strips were impregnated with ceftazidime/ceftazidime + clavulanic acid (0.64–4 μg/mL), ceftazidime/ceftazidime + clavulanic acid (0.16–1 μg/mL) and the MIC value was quantified in μg/mL (CLSI Guidelines, 2016) [31]. For MIC stripe method, each strip between the inhibition eclipse and zone of edge in the strips containing points were recorded as MIC. If the ESBL production show positive result, the microbial isolates exhibited an MIC zone in >0.5 for cefotaxime, >1 for ceftazidime; and >8 for cefotaxime/cefotaxime + cefotaxime/clavulanic acid or ceftazidime/ceftazidime + clavulanic acid [32].

2.6. Antibacterial activity

The antibacterial properties of the resultant Ag NPs, CS/Ag NCs were tested against ESBL producing *P. aeruginosa* using agar well diffusion method previously reported [33]. Briefly, an overnight grown culture of ESBL producing *P. aeruginosa* was spread on muller hinton agar plates (MHA) using sterile cotton swabs. The wells were cut into the medium and various concentrations of Ag NPs, CS/Ag NCs were added. Third-generation cephalosporin disc (ceftazidime, 30 μg) acted as a positive control for ESBL production and distilled water served as a negative control. The plate was incubated at 37 °C for 24 h. After incubation, the inhibition zone around the wells was measured in diameter (mm) and the resulting zones were compared with negative control of the distilled water wells. The absence or presence of the positive control disc around the zone was also measured for detection of ESBL production.

2.6.1. Minimum inhibition concentration

The MIC and MBC of Ag NPs, CS/Ag NCs against ESBL producing *P. aeruginosa* were determined using microdilution method using Luria bertani broth (LB) [34]. In brief, 10 μL of bacterial strain was inoculated into the previously filled 100 μL of sterile LB broth containing 96 well plates. After, increasing concentration 10, 20, 30, 40, 50, 60, 70, 80, 90, 100 μg/mL of Ag NPs, CS/Ag NCs (the ultra sonication was made for pure suspension of particles and it acts as a dissolved solution, which accurately reflects the amount of Ag NPs, CS/Ag NCs available in solution to act on the *P. aeruginosa*) was filled into the respective wells. The final volume of the 96-well was 300 μL. The bacterial culture alone in the sterile broth of the well acted as a control. The plate was incubated at 37 °C for 24 h. After incubation, the MIC value was identified by checking the turbidity of the bacterial growth. The MIC value corresponded to the concentration that inhibited 99% of the tested bacterial growth and their optical densities of the plate were read with a UV–Vis spectrophotometer at a wavelength of 570 nm for inhibition of growth level quantification. The work was performed in triplicate and the percentage of inhibition was calculated by using the formula,

$$\text{Inhibition}\ (\%) = ((\text{Control OD 570 nm} - \text{Test OD 570 nm})/\text{Control OD 570 nm}) \times 100$$

2.6.2. Minimum bactericidal concentration

The MBC of Ag NPs and CS/Ag NCs against ESBL producing *P. aeruginosa* was assessed according to a conventional method [35]. Briefly, an aliquot of 10 μL from all the MIC wells, which showed decreased bacterial growth was inoculated in MHA plates without addition of any nanomaterial and then incubated at 37 °C for 24 h. The antibacterial inhibition of Ag NPs and CS/Ag NCs were considered when either MIC and MBC values were equal or when MBC was higher than MIC [20].

2.6.3. Confocal laser scanning electron microscope

The potential MIC concentration of Ag NPs and CS/Ag NCs induced intracellular damage in ESBL producing *P. aeruginosa* was analyzed by CLSM [36]. Briefly, the log phase culture of ESBL producing *P. aeruginosa* was treated with MIC of Ag NPs, CS/Ag NCs into the tryptic soy broth (TSB) containing a 24 well plate. Non-treated Ag NPs and CS/Ag NCs containing *P. aeruginosa* well acted as a control and the plate was maintained at 37 °C for 24 h. After incubation, both the test and control samples were centrifuged at 10000 rpm for 15 min to promote better mode of action of the pellets. 10 μL of acridine orange-ethidium bromide (AO/EB) were used to stain with each pellet-containing tube. Finally, the samples were smeared on a glass slide and covered with cover slides. The cell death of the Ag NPs, CS/Ag NCs treated ESBL producing *P. aeruginosa* or live cells of the tightly arranged non-treated control sample of the glasses were separately observed by CLSM. The samples were imaged using a Carl Zeiss CLSM 710 (Carl Zeiss, Jena, Germany) equipped with a 100 × oil-immersion objective lens.

2.6.4. Scanning electron microscope

The Ag NPs and CS/Ag NCs non-treated or treated ESBL producing *P. aeruginosa* morphological differentiation was observed by SEM [37]. Briefly, the 12 h culture of ESBL producing *P. aeruginosa* was treated with MIC of Ag NPs, CS/Ag NCs and incubated at 37 °C for 12 h. After incubation, the treated samples were centrifuged at 5000 rpm for 30 min and then cell suspensions were fixed with 4% glutaraldehyde millonig's phosphate buffer (pH 7.3) for 4 h, followed by three time washing in the same buffer. The fixed cells were vacuum filtered using polycarbonate membrane filters and dehydrated with ethanol-graded series (10, 20, 30, 40, 50, 60, 70, 80, 90 and 100%). The dehydrated samples were allowed to air dried and mounted onto aluminum stubs and coated using gold-palladium metal (60:40 alloys) with 15 nm thickness. Finally, the samples were air-dried and analyzed using a Cambridge Stereo scan 200 scanning electron microscope (model: VEGA3 TESCAN, Brno, Czech Republic) using an accelerating voltage of 20 kV.

2.7. Anti-β-lactamase activity by iodimetric assay

Anti-β-lacamase effect of Ag NPs and CS/Ag NCs against ESBL producing *P. aeruginosa* was assessed by microiodimetric assay using 24-well plate [38]. Briefly, the log phase culture of ESBL producing *P. aeruginosa* was added into TSB with MIC of Ag NPs, CS/Ag NCs in 24-well plate at 37 °C and incubated overnight and supplemented with amoxicillin to stimulate β-lactamase secretion. After incubation, the sample was centrifuged by 5000 rpm for 30 min. After centrifugation, the pellet was collected and resuspended in phosphate buffer at pH 7 with iodine solution and the sample was incubated for 1 h. After incubation, the cells were lysed using an ultrasonicator followed by addition of starch-iodine reagent. After 30 min incubation, the color change was monitored, as expected due to the reaction of iodine with starch. After 10 min incubation, the blue color of the well containing amoxicillin indicated that beta-lactam ring cleavage did not occur. The quick decolorization of the sample indicate that amoxicillin molecules are being hydrolyzed and the amoxicillin play a role in the beta-lactamase inhibition activity. A microdimetric assay was carried out separately after preincubating the bacterial cells using various concentrations (10–100 μg/mL) of Ag NPs and CS/Ag NCs in starch iodine

solution to determine anti-β-lactamase activities in 24-well plate. All the plates were incubated at 37 °C for 24 h. The optical density (OD) of starch-iodine solutions was measured based on the color changes at 630 nm using a microplate reader (Rayto, China).

2.8. In-vivo toxicity effect of Ag NPs and CS/Ag NCs against A. fanciscana

The in-vivo toxicity effect of Ag NPs and Ag/Cs NCs were assessed against brine shrimp adult *A. fanciscana* as described before in the literature [39]. The natural seawater was collected from sea and filtered through a 50 μm net to remove the organic matters and maintained seawater salinity at 35 ppt. This salt water was oxygenated using a common air pump that is used in ornamental fish culture. The temperature and pH were adjusted within the ranges of 26–29 °C and 7.5–8.5, respectively, in a control room. Commercial brand GSI (Great Salt Lake) *A. franciscana* cyst was hatched out in salt water and maintained in stock culture under laboratory condition as reported before in the literature [40]. The Ag NPs and Ag/Cs NCs were solubilized in a proportion of 0.5 mL to 2 mL and saline solution was taken to obtain stock solution at concentration of zero (0). Fold dilutions of 10, 20, 30, 40, 50, 60, 70, 80, 90 and 100 μg/mL were used to achieve the detection of mortality. Each 30 adult *Artemia* were released in experimental setup. The experiments were protected from light for 24 h and experiments were performed in triplicate. After 24 h, the number of dead individuals was counted (eg. inactive condition) using a magnifying glass. The study of sample toxicity was rated based on the adult *Artemia* death, which was classified by observing the absence of swimming activity in the experimental samples. The toxicity level was considered as follows; 10 μg/mL concentration as nontoxic; 50 μg/mL as moderate toxics and above 60 μg/mL as highly toxic for Ag NPs and Ag/Cs NCs. Further, the mortality ability of Ag NPs and Ag/Cs NCs was further assessed by light microscope analysis to observe the internal organs of the *A. franciscana*. The affected *A. franciscana* was recovered with a net and dissected very carefully with sterile scalpel. The affected parts of the intestine were collected separately, and the morphological damages were observed using a light microscope using crystal violet stain.

3. Results and discussion

3.1. Synthesis and characterization of nanomaterials

Typical UV–Vis absorption spectra of Ag NPs and CS/Ag NCs are shown in Fig. 1a. The spectrum corresponding to the Ag NPs sample display the distinctive surface plasmon resonance (SPR) absorption peak located at a wavelength of ~423 nm, suggesting the successful synthesis of Ag NPs [41]. This result suggests that the concentration of reducing agent in the reaction solution and temperature play a significant role for during the reduction procedure for Ag NPs synthesis. This agrees with earlier findings regarding Ag NPs synthesis [42,43]. In the present work, CS/Ag NCs were prepared at 90 °C and the starting solution experienced a color variation from colorless to yellow color within 60 min. UV–Vis spectrophometry revealed a peak located at a wavelength of ~430 nm, related to the synthesis of CS/Ag NCs (Fig. 1a). When comparing spectra obtained for Ag NPs and Cs/Ag NCs, the intensity of the absorption peak of CS/Ag NCs decreases (Fig. 1a red line) upon addition of Ag NO_3 in the CS solution. At same time, the position of the absorption peak was found to shift towards a higher wavelength, from ~423 to 430 nm. During CS/Ag NCs synthesis, most of Ag^+ ions chemically

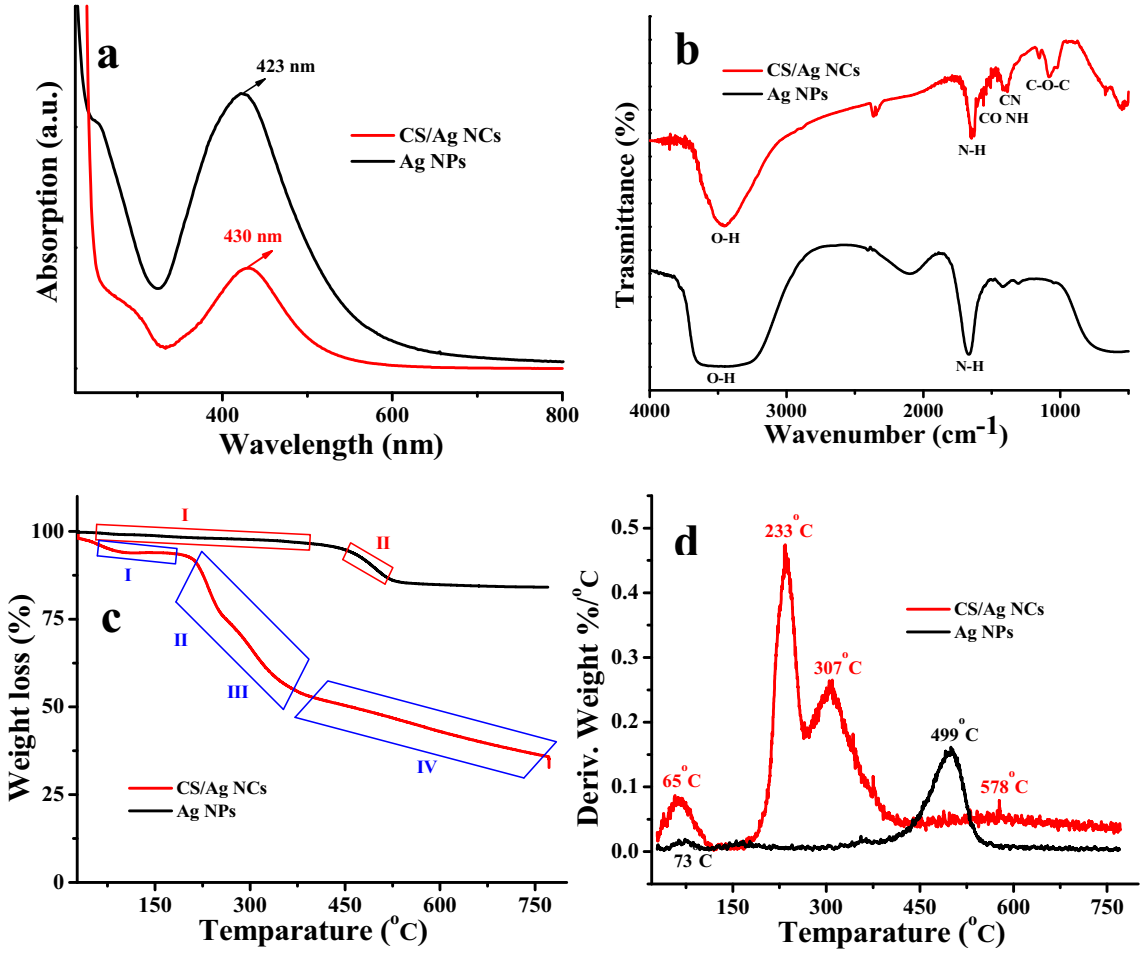

Fig. 1. UV–Vis absorption spectra (a), FTIR spectra (b), TGA traces (c) and DTA (d) for Ag NPs (black line) and CS/Ag NCs (red line).

interact with acetic acid, which participate in the formation of CS/Ag NCs [44].

FTIR spectra for Ag NPs and CS/Ag NCs are shown in Fig. 1b. These provide information on the molecular structure of Ag NPs and Ag NPs to CS. The FTIR spectrum of the Ag NPs shows absorption peaks located at wavenumber positions of ~3531 and 1674 cm^{-1}, which corresponds to O—H stretching and N—H bending vibrational motions, respectively (Fig. 1b block line). This finding is in agreement with our results published earlier [45]. The FTIR spectrum of CS/Ag NCs shows absorption peaks located at wavenumber positions of ~3464, 1643, 1536, 1384 and 1062 cm^{-1}, which correspond to O—H stretching, N—H bending, N—H angular deformation in C—O N—H plane, C—N band and C—O—C band stretching vibrational motions, respectively. This result agrees with our previous report that also involved the synthesis of CS/Ag NCs [30]. The absorption peak located at a wavenumber position of ~1062 cm^{-1} more particularly provides information on the interaction between Ag NPs and the amino groups of CS. When comparing the spectra of Ag NPs and CS/Ag NCs, the CS/Ag NCs from Fig. 1b, several shifts towards higher or lower wavenumber are observed. The peak located initially at ~3531 cm^{-1} (for Ag NPs) shifts to a wavenumber position of ~3464 cm^{-1} (for CS/Ag NCs). Other peak shifts from ~1674 cm^{-1} (for Ag NPs) down to ~1643 cm^{-1} (for CS/Ag NCs), which was also accompanied by a decrease in absorption intensity. The CS/Ag NCs spectra indicate that the vibrational motions of N—H moieties that belong to the molecular structure of CS was somehow disturbed by the presence of Ag NPs in contact with CS. These changes may be due to the interaction of OH groups with Ag^{+} ions [46]. In our previous report, FTIR spectra of CS/Ag NCs suggested similar information [30].

The thermal stability of Ag NPs and CS/Ag NCs was assessed using TGA analysis. TGA traces for these materials are shown in Fig. 1c. First of all, the TGA trace corresponding to Ag NPs show a weight loss of ~2.9% from ~57 up to 430 °C (stage I). This weight loss may occur due loss of water molecules and impurities (Fig. 1c block line). This stage of weight loss was relatively small amount, which suggest that relatively highly pure Ag NPs were successfully synthesized. A second weight loss of ~10.4% is observed (stage II) from ~439 up to 530 °C. This relatively small weight loss might be associated to the thermal degradation of organic components. The TGA trace of CS/Ag NCs shows three weight loss stages. The first weight loss of ~6.1% (stage I) starts from ~49 °C up to ~157 °C, which may be related to loss of water molecules and volatile impurities from the sample (Fig. 1c red line). A second weight loss of ~37% (stage II and III) can be seen, which starts from ~204 up to 375 °C. This weight loss has been reported to be due to the thermal degradation of amine and —CH_2OH assembly that belong to the molecular structure of CS [47]. A fourth weight loss can be observed, which starts from ~402 up to 773 °C. This weight loss has been reported to occur due to the degradation of glucopyranose of [48].

DTA curves of Ag NPs and CS/Ag NCs have conformed polar groups and consequently water can be simply adsorbed by hydrogen bonding [49]. The two peaks of DTA curve of Ag NPs was indicated the first and second degradation stages (Fig. 1d black line). First degradation temperature of Ag NPs is at 73 °C, for water molecules burning temperature and the second degradation temperature is at 499 °C for the organic components' temperature. The second stage of degradation temperature, peaks are broader with higher intensity. The four peaks of DTA curve of CS/Ag NPs was indicated the degradation temperature at 65 °C, 233 °C, 307 °C and 578 °C, for water molecules burning temperature, amine, primary alcohol temperature and carbonization temperature (Fig. 1d red line). It reveals that with increased amounts of silver particles into the chitosan matrix lead to enhanced thermal stability.

The powder XRD pattern of Ag NPs is shown in Fig. 2 (black line). Four main diffraction peaks located at 2θ positions of ~38.1°, 44.2°, 64.5, and 77.3° can be observed, which correspond to the (111), (200), (220) and (311) crystalline, respectively. This pattern was found to be an almost perfect match with the JCPDS card no. 040783 [50]. This suggests the successful synthesis of crystalline and pure Ag

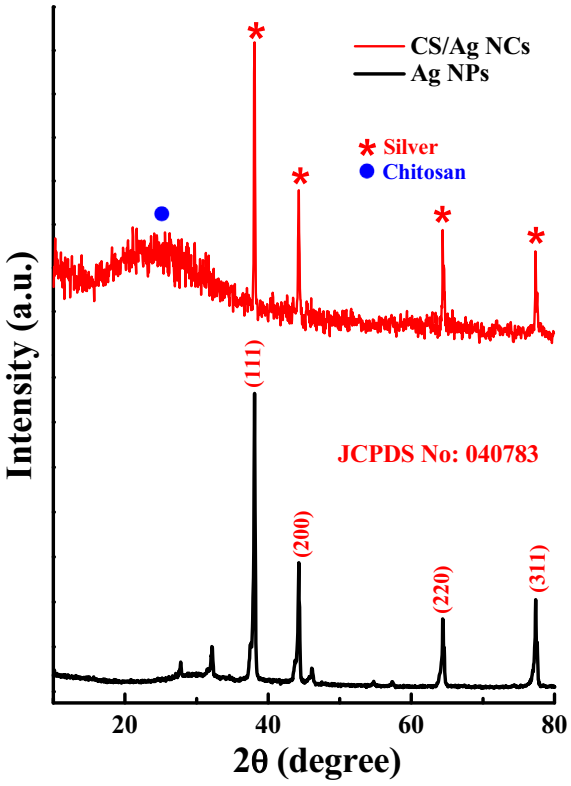

Fig. 2. Powder XRD pattern of Ag NPs (block line) and CS/Ag NCs (red line).

NPs. The powder XRD pattern for CS/Ag NCs is reported in Fig. 2 (red line). One can observe diffraction peaks that occur due to the presence of CS and Ag NPs This observation agrees with the values reported in our earlier report on CS/Ag NCs [30]. For the pattern, corresponding to CS/Ag NCs (Fig. 2), the broad diffraction peaks from CS is highlighted with a blue dot, while the diffraction peaks occurring from the presence of Ag NPs are highlighted using red stars. The broad diffraction peak of CS is located at a 2θ value of ~25.3°, which is typical of an amorphous polymer. Diffraction peaks of Ag NPs are found to occur at 2θ values of ~37.9°, 44.3°, 64.5° and 77.4°. The powder XRD pattern obtained for the CS/Ag NPs was found to be consistent with the monoclinic crystalline morphology of Ag NPs, even when these are embedded into a CS matrix. As expected, the intensity of the diffraction peaks that occur due to the presence of Ag NPs in CS/Ag NCs were found to decrease when Ag NPs are embedded in the CS matrix (Fig. 2 block line). The powder XRD pattern obtained for CS/Ag NCs does not contain any additional diffraction peaks, suggesting that no contamination was present in the CS/Ag NCs. This result agrees with the previously discussed TGA data, which also suggested that high purity materials have been synthesized.

The surface morphology of the synthesized Ag NPs and CS/Ag NCs was examined by TEM analysis. The corresponding images are shown in Fig. 3. TEM micrographs of Ag NPs show that the particles were closely packed and possess sphere-like morphology as well as nanosized dimensions (Fig. 3a,b). The sphere-like morphology and size of the synthesized Ag NPs was found to be relatively uniform with size ranging from 10 up to 35 nm. The TEM images (Fig. 3c,d) of CS/Ag NCs confirmed that the NCs possess two phases, one being CS and the other Ag NPs, due to their different densities, which results in generating contrasts. The Ag NPs were found to form aggregates, which are surrounded by the CS matrix [51]. During the reduction process, the agglomeration of Ag NPs may occur due to diffusion effects, while the CS matrix was allowed to dissolve for extensive time. For CS/Ag NCs, Ag NPs aggregates were surrounded by the CS matrix and the Ag NPs were found to possess dimensions in the nanosized range. The size of

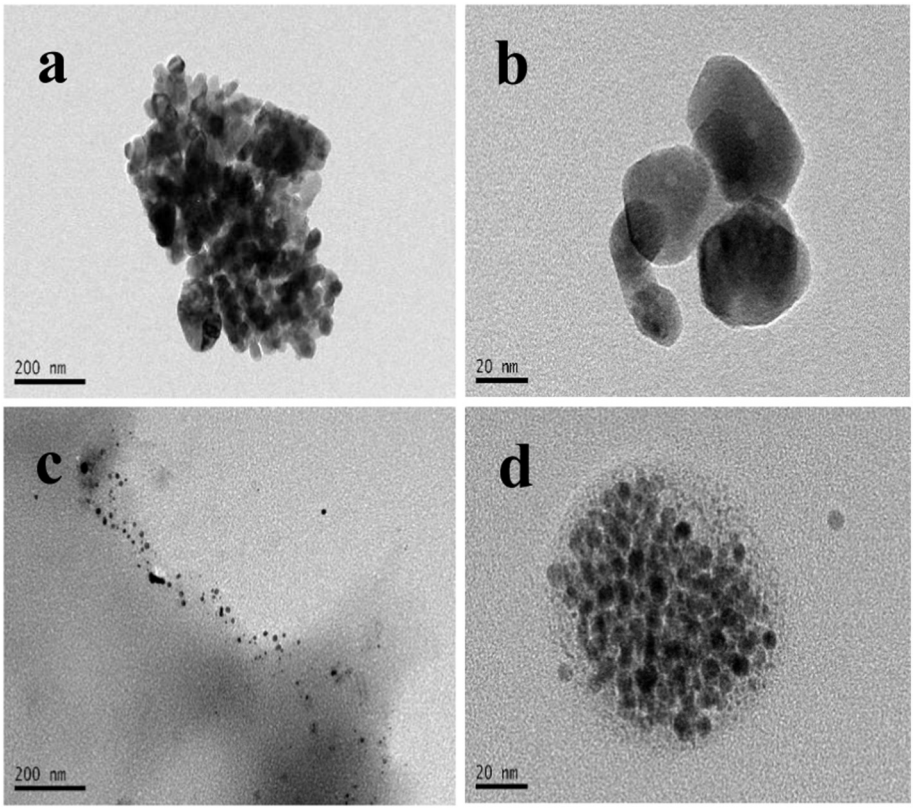

Fig. 3. TEM micrographs of Ag NPs (a,b) and CS/Ag NCs (c,d).

the Ag NPs that formed these aggregates embedded in the CS matrix were found to range from 6 up to 18 nm. Compared with Ag NPs synthesized without CS, the Ag NPs obtained with the presence CS were smaller (Fig. 3). This observation may be related to the stabilizing effect of CS during the reduction reaction.

3.2. Detection of MDR effect of P. aeruginosa

Based on the rod shaped Gram-negative, motile colonies of the 10 collected strains were morphologically recorded by oil immersion lens of light microscope. The positive oxidative and cetrimide result confirmed that the tested strains were *P. aeruginosa*. After confirmation, all the strains were named as BDU 1, BDU 2, BDU 3, BDU 4, BDU 5, BDU 6, BDU 7, BDU 8, BDU 9, BDU 10. Among the 10 strains of *P. aeruginosa*, BDU 1, BDU 3 and BDU 5 exhibited more resistance against almost all tested HEXA disc containing antibiotics. The BDU 2 and BDU 4 strains also developed resistance against most of the HEXA disc antibiotics, except against ciprofloxacin, piperacillin/tazobactam and cefoperazone/sulbactum (Table 2). The BDU 2 and BDU 4 strains exhibited 20 mm, 19 mm, 17 mm, and 20 mm 18 mm 17 mm inhibition zone, respectively. On the other hand, BDU 6, BDU 7, BDU 8, BDU 9 and BDU 10 were found to be generally more sensitive to antibiotics. Based on the highest degree of resistance, the BDU 5 strain exhibited smaller inhibition zone against all the tested antibiotics, compared to BDU 1 and BDU 3 strains. The zone did not exceed the standard zone level of CLSI guidelines. The BDU 1 and BDU 3 strains exhibited 14 mm, 16 mm inhibition zone against ciprofloxacin, 19 mm, 21 mm against piperacillin/tazobactam and 18 mm, 19 mm against cefoperazone/sulbactum, respectively. These values were found to be a little high compared to the BDU 5 strain. In particular, the selected *P. aeruginosa* BDU 5 strain developed resistance against carbapenems such as imipenem, meropenem and ertapenem, which showed no inhibition zone against tested antibiotics. This result was found to correlate with the WHO report [1] where the selected *P. aeruginosa* BDU 5 was reported for its carbapenems resistance character. The exhibited zones of the antibiotics could not complete their role against selected *P. aeruginosa* BDU 5 strains by target site modification. It revealed that the zone producing antibiotics were ineffective against BDU 5, due to the minimum level of inhibition (CLSI guidelines, 2016). The Hexa discs zone interpretation was compared with CLSI guidelines against *P. aeruginosa* and is summarized in Table 1. Hence, our result demonstrated that the *P. aeruginosa* BDU 5 strain is a MDR uropathogens, especially carbapenems resistant and it developed resistant against all the current antibiotics, which may lead to ESBL production. The MDRs of the *P. aeruginosa* BDU 5 strain against tested HEXA discs are shown in Fig. 4a–d. The zone variations of BDU 1, BDU 3 and BDU 5 strains against tested HEXA discs are presented in Table 2. The results obtained in the present study agree with our earlier findings [52]. A previous study reported that 80% of UTI pathogens developed resistance to antibiotics due to the unusual environment due to unprescribed and over use of antibiotics [53]. In our recent report, minimum zone of HEXA discs antibiotics against GNB developed resistance against tested antibiotics (CLSI guidelines) meaning that it could not be used against any infections due to the previous usage failure [54].

3.3. Detection of carbapenems resistant ESBL producing P. aeruginosa

After 24 h incubation of the carbapenems resistant *P. aeruginosa* BDU 5 strain with Hexa G-minus 24 disc antibiotics, results revealed no inhibition zone around all the discs, except with cefotaxime where a 14 mm inhibition zone was produced (Fig. 4e). Clearance zones within >22 mm for ceftazidime, >27 mm for cefotaxime, >21 mm for cefpodoxime and no zone of double discs in the cefpodoxime/clavulanic acid, ceftazidime/clavulanic acid, cefotaxime/clavulanic acid were observed and as a result, the BDU 5 strain was considered as ESBL producer (CLSI Guidelines). The *P. aeruginosa* BDU 1 and BDU 3 strains exhibited 14, 24, 20 mm and 13, 20, 22 mm clearance zone against ceftazidime, cefotaxime and cefpodoxime, respectively. The increasing zone of 5 mm of cefpodoxime/clavulanic acid, ceftazidime/clavulanic acid and

Table 1
The Hexa discs zone interpretation chart against *P. aeruginosa* based on the CLSI guidelines.

S. no	Antibiotics	CLSI guidelines for MDRs of enterobacteriacea (CLSI)			Test pathogens
		S (mm)	I (mm)	R (mm)	
1	Ceftazidime (CAZ-30 μg)	21	18–20	19	*P. aeruginosa*
2	Cefotaxime (CTX-30 μg)	24	21–23	20	*P. aeruginosa*
3	Ciprofloxacin (Cip-5 μg)	21	16–20	15	*P. aeruginosa*
4	Co-Trimoxazole (Cot-25 μg)	16	11–15	10	*P. aeruginosa*
5	Gentamycin (GEN-10 μg)	13	9–11	10	*P. aeruginosa*
6	Imipenom (IMP-10 μg)	26	23–25	22	*P. aeruginosa*
7	Ticarcillin/clavulanic acid (TCC-75/10 μg)	24	21–23	21	*P. aeruginosa*
8	Meropenem (MRP-10 μg)	26	21–22	22	*P. aeruginosa*
9	Ertapenem (ETP-10 μg)	20	17–19	21	*P. aeruginosa*
10	Cefoperazone/sulbactum (CFS-75/10 μg)	22	13–16	13	*P. aeruginosa*
11	Piperacill/tazobactam (PIT-100/10 μg)	23	14–17	14	*P. aeruginosa*
12	Nalidixic acid (NA-30 μg)	23	18–21	13	*P. aeruginosa*
13	Ampicillin (AMP-30 μg)	22	17–19	12	*P. aeruginosa*
14	Cephalothin (CEP-30 μg)	22	22–23	16	*P. aeruginosa*
15	Ampicillin (AMP-10 μg)	18	14–17	13	*P. aeruginosa*
16	Aztreonam (AT-10 μg)	18	14–17	13	*P. aeruginosa*
17	Norfloxacin (NF-10 μg)	17	13–16	12	*P. aeruginosa*
18	Netillin (NET-10 μg)	16	12–14	10	*P. aeruginosa*

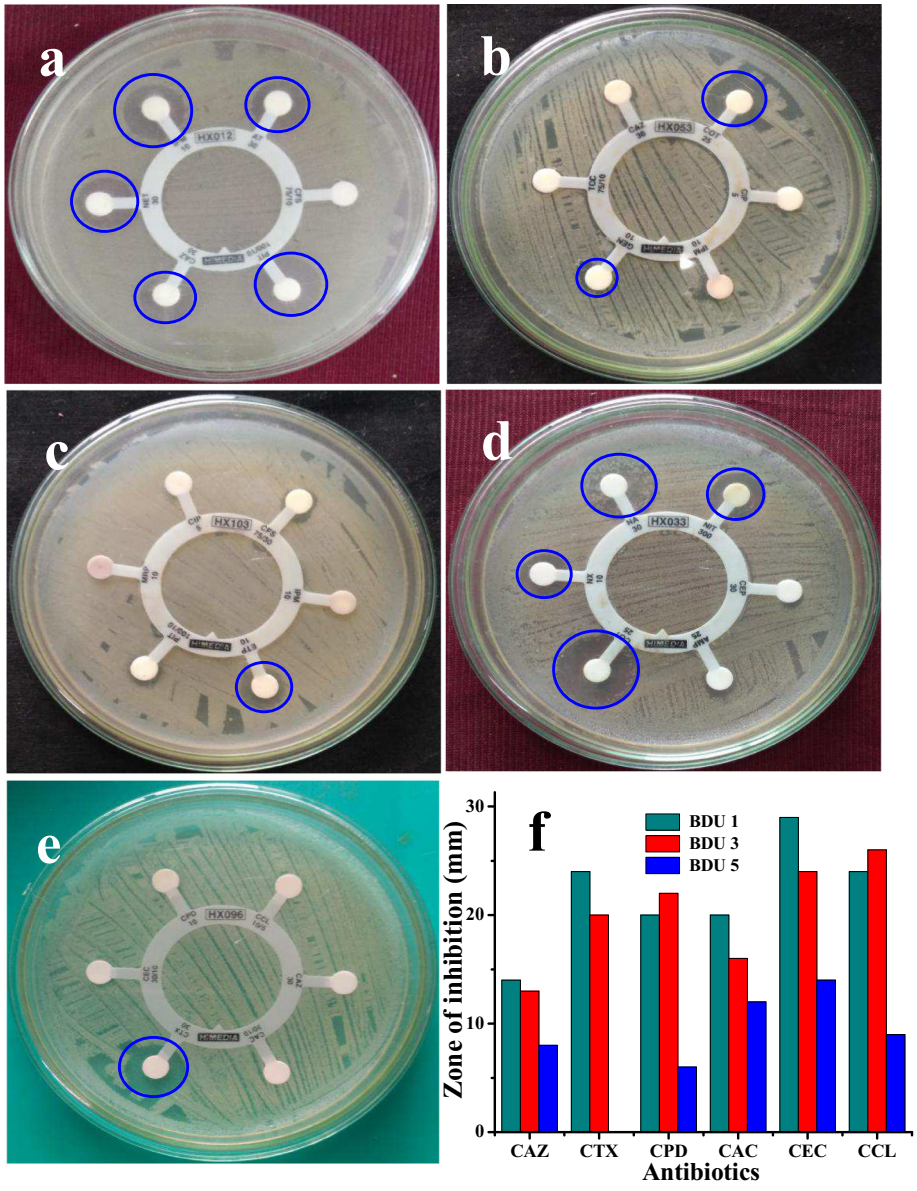

Fig. 4. Detection of multi drug resistant (a-d), detection of ESBL production in *P. aeruginosa* BDU 5 by HEXA dis method (e), inhibition zone variation of BDU 1, BDU 3 and BDU 5 strains (f).

Table 2
Detection of MDRs effect in *P. aeruginosa* by specific HEXA Discs for *P. aeruginosa*.

S. no	Antibiotics	BDU 1	BDU 2	BDU 3	BDU 4	BDU 5
1	Cefoperazone/sulbactum (CFS)	18	14	19	17	4
2	Piperacillin/tazobactam (PIT)	19	17	21	20	4
3	Ticarcillin/clavulanic acid (TCC)	4	10	11	9	5
4	Co-trimoxazole (COT)	0	14	12	0	6
5	Ciprofloxacin (CIP)	14	20	16	19	2
6	Nitrofurantoin (NT)	0	0	8	0	0
7	Nalidixic acid (NA)	2	0	8	0	2
8	Cephalothin (CEP)	0	6	7	0	0
9	Ampicillin (AMP)	0	8	9	0	0
10	Norfloxacin (NX)	4	0	0	0	2
11	Meropenem (MRP)	0	0	0	8	0
12	Ceftazidime (CAZ)	6	0	0	6	2
13	Cefotaxime (CTX)	0	4	0	4	0
14	Ertapenem (ETP)	2	0	0	3	2
15	Gentamycin (GEN)	0	0	0	6	2
16	Aztreonam (AT)	0	0	9	10	2
17	Imipenom (IPM)	0	0	6	10	9
18	Netillin (NET)	2	0	8	10	6

cefotaxime/clavulanic acid was also observed against both the BDU 1 and BDU 3 strains. Based on the CLSI Guidelines, all the results suggested that the *P. aeruginosa* BDU 1, BDU 3 and BDU 5 strains were ESBL producers. In particular, carbapenems resistant *P. aeruginosa* BDU 5 was more resistant to all the tested antibiotics than any other and were confirmed by phenotypic identification method. The inhibition zone variation of BDU 1, BDU 3 and BDU 5 is shown in Fig. 4f. Among the 3 strains, the carbapenems resistant *P. aeruginosa* BDU 5 strain was easily susceptible to other infections like obstruction of UTI, blockage of urinary catheters, bladder, kidney stone and bacteriuria [55]. A previous study suggested that *P. aeruginosa* is the second most ESBL producing bacteria. Its MDR behavior is often attributed to patient-to-patient transmission of resistant strains as well as newly acquired resistance owing to previous antibiotic exposure [13]. Recently, another study reported that the MDR of *P. aeruginiosa* is non-susceptible to at least one antibiotic in three or more antimicrobial categories [56]. The Hexa disc result, however, confirmed that the isolated *P. aeruginosa* strains of BDU 1, BDU 3 and BDU 5 are ESBL producers and possess enhanced ability against all current antibiotics.

In addition, the HEXA disc method of ESBL positive *P. aeruginosa* strains of BDU 1, BDU 3 and BDU 5 was further confirmed by combination MIC *E*-stripe method. The E-stripe produced 0.38, 0.40, 0.36 mm zones of inhibition for ceftazidime/ceftazidime + clavulanic acid and 0.34, 0.39, 0.42 mm zones for cefotaxime/ceftazidime + clavulanic acid against BDU 1, BDU 3 and BDU 5 strains, respectively. Interestingly, carbapenems resistant *P. aeruginosa* BDU 5 exhibited the lowest zone of inhibition than the two strains against ceftazidime/ceftazidime + clavulanic acid cefotaxime/ceftazidime + clavulanic acid as observed in Fig. 5a–b. On the contrary, no inhibition zone on the opposite end of the MIC-stripe containing ceftazidime and cefotaxime was observed against the three *P. aeruginosa* strains. The test result confirmed the zone of inhibition is below the range of MIC >8 mm value. Therefore, the MIC-stripe method cardinally indicates that the selected bacterial strains were ESBL producer (CLSI guidelines, 2016). The inhibition zone variation of MIC stripe against BDU 1, BDU 3 and BDU 5 strains is reported in Fig. 5c. The MIC stripe result revealed that *P. aeruginosa* strains developed resistance against maximum level of antibiotic usage [57]. Based on the complete resistance characteristic features of the carbapenems resistant *P. aeruginosa* BDU 5 strain against all the tested antibiotics, it was chosen for this study. Our result was found to agree with previous reports [2,58] where the MIX + stripe result exhibited 0.32, 0.39 mm zone against ESBL producing *P. aeruginosa* and *K. pneumoniae*, respectively. On February 2017, the WHO stated that three types of resistance pathogens are “critical” such as carbapenems, imipenem and fluoroquinolones [59]. The range of MIC value was >8 mm, which is a positive result for ESBL production in Gram-negative bacteria (CLSI guidelines) as previously evidenced [60]. The exhibited result confirmed that the carbapenems resistant *P. aeruginosa* BDU 5 strain has the multi drug resistant ability that leads to ESBL production. Hence, there is an emerging need to identify new types of antibacterial agents to eradicate infections generated by *P. aeruginosa*. Furthermore, there is a high demand for novel strategies to detect the appropriate inhibitors against ESBL producing pathogens and β-lactamase, which has been very challenging. During the past few years, the emergence of CS/metal NCs and its efficiency against various antibiotic resistance infections have shown promises.

3.4. Antibacterial activity

Based on its ESBL producing ability, the carbapenems resistant *P. aeruginosa* BDU 5 strain was chosen for this study and identify its inhibition ability using synthesized Ag NPs and CS/Ag NCs. After 24 h incubation, the Ag NPs and CS/Ag NCs treated carbapenems resistant *P. aeruginosa* BDU 5 strain showed 16 mm and 20 mm zone of inhibition at concentrations of 80 μg/mL and 50 μg/mL, respectively. The minimum 7 mm and 11 mm zone of inhibition was observed at a concentration of 25 μg/mL for both materials. The result revealed that the CS/Ag NCs possess more antibacterial efficiency than Ag NPs alone. On the other hand, the positive control of ceftazidime for ESBL production showed 10 mm zone and distilled water did not exhibit zone of inhibition (Fig. 6a–c). Here, the viability of the carbapenems resistant *P. aeruginosa* BDU 5 strain decreased due to the presence of silver ions. The outer membrane of the *P. aeruginosa* is covered by lipopolysaccharides and is electrostatically linked with divalent bond that produces a stable structure at the surface of the outer membrane [61]. This bonding region is a weak binding site of the outer membrane for Ag^+ ions. Ag^+ ions, however, easily bind to this region of outer membrane and form various complex reactions with nitrogen and other substituents. This is how Ag NPs effectively damage the lipopolysaccharides and collapse the outer membrane of the target cell [62]. The inhibition ability of NPs can be further improved by polymers including CS, gelatin, collagen etc. [63,64]. Polymers may offer a promising solution as they can also act as a carrier for antibiotics, NPs and natural compounds [65]. The most successful research evidence of the excellent activity of CS/Ag NCs against efflux pumps, biofilms biofilm, quorum sensing and β-lactamase production in MDR producing bacterial pathogens has been report in a previous study [66]. An important current issue of CS/Ag NCs is to overcome their toxicity in MDR bacteria [67].

3.4.1. Minimum inhibition concentration

After 24 h incubation, the strong dose-dependent antibacterial activity of Ag NPs and CS/Ag NCs treated ESBL positive carbapenems resistant *P. aeruginosa* BDU 5 culture was observed at various concentrations. The strongest growth decrease of *P. aeruginosa* showed 76 and 92% of inhibition at 80 μg/mL and 50 μg/mL of Ag NPs and CS/Ag NCs, respectively (Fig. 6b). It was found that, as the concentration of Ag NPs and CS/Ag NCs increases, the growth of carbapenems resistant *P. aeruginosa* BDU 5 also decreases. This result reflected that the MIC of both nanomaterials has potential in fighting the growth of carbapenems resistant *P. aeruginosa* BDU 5 at increasing concentration. After 12 h incubation, the initiation of inhibition was not reached for Ag NPs treated *P. aeruginosa* until a 25 μg/mL concentration was used. No minimum time was required for CS/Ag NCs to achieve desired inhibition effect. CS/Ag NCs initiated their role against *P. aeruginosa* at a concentration of 5 μg/mL. The result revealed that both nanomaterials were effective against the chosen carbapenems resistant *P. aeruginosa*, but that CS/Ag NCs were even more efficient that Ag NPs.

3.4.2. Minimum bactericidal concentration

The desired MIC was validated by MBC to avoid any misinterpretation. All the turbidity of insoluble MIC solution was suppressed by dilution on the MHA plates. After 24 h incubation, the inhibition

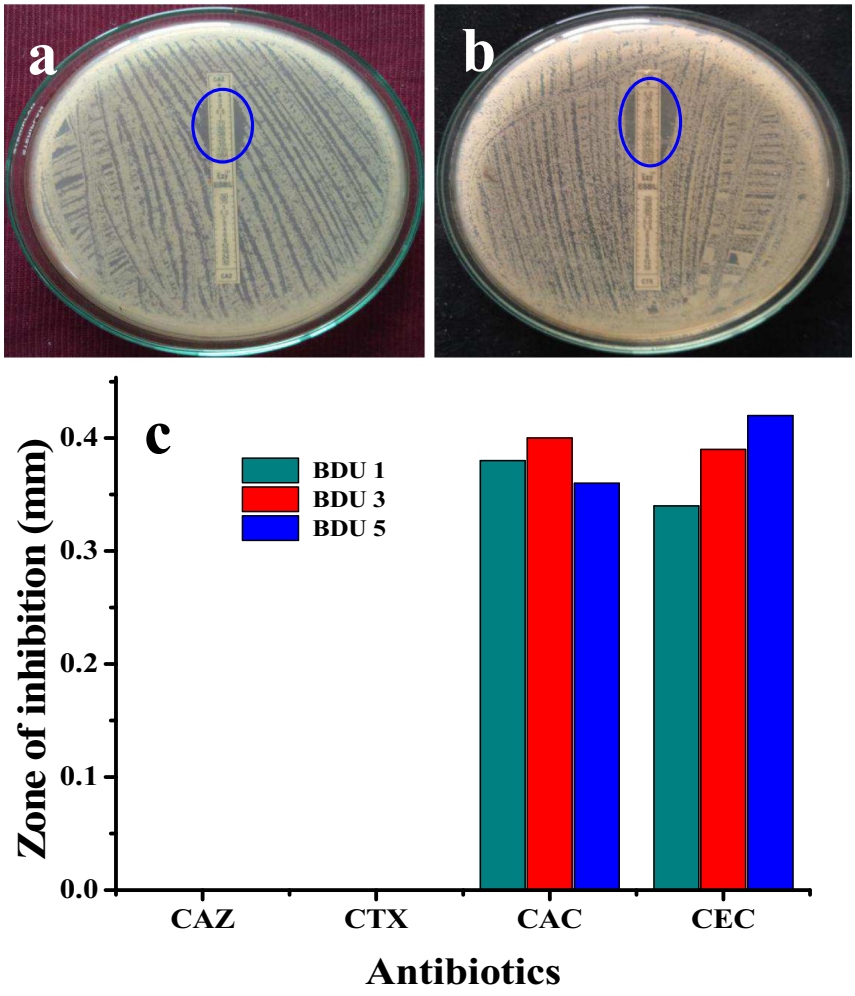

Fig. 5. MIC stripe method variation of HEXA disc method of ESBL detection (a, b) and inhibition zone variation of MIC stripe (c) against BDU 1, BDU 3 and BDU 5 strains.

concentration of both nanomaterial concentrations was noted, where no visible growth appears on the MHA plate when nanomaterial treatment was utilized. The MBC result exhibited similar MIC of Ag NPs and CS/Ag NCs in treated carbapenems resistant *P. aeruginosa* BDU 5 in diluted MBC plate (6 d, e). Hence, both MIC and MBC results were confirmed meaning that concentrations of 80 μg/mL and 50 μg/mL of Ag NPs and CS/Ag NCs have the potential to inhibit ESBL producing *P. aeruginosa* and these concentrations was used as a MIC for further inhibition study.

The identified results of MIC and MBC suggest that the growth of the carbapenems resistant *P. aeruginosa* BDU 5 strain stopped in the log phase due to the intracellular penetration of both nanomaterials, acting as bactericidal agents, into the bacterial cells that altered their bacterial activity [68]. The results can be clearly explained on the basis of the differences in the cell wall of *P. aeruginosa*. The cell wall of GNB is made up of peptidoglycan layer, which acts a selective permeability barrier to protect bacteria from harmful agents, such as drugs, toxins, and degradative enzymes and penetrating nutrients to sustain bacterial growth [69]. The structure and chemical nature of the outer cell membrane in *P. aeruginosa* arranged in lipid bilayer and the presence of phospholipid chains act as a potential barrier to GNB [70]. Our result suggests that Ag NPs and CS/Ag NCs may alter the outer membrane of the lipopolysaccharide at desired MIC. The altered outer membrane of *P. aeruginosa* possesses rough surface, mucoid or butyrous damage due to the external cleavage of cell wall. The accumulation of the nanomaterial inside the bacterial cell was shown due to blockage of bactericidal effect and protein synthesis mediated by the 30S ribosomal subunit or nucleic acids synthesis [71]. The inner and outer membrane damage result of Ag NPs and CS/Ag NCs treated *P. aeruginosa* morphology was clearly visualized by CLSM and SEM images. Previous MIC reports of Ag NPs and CS/Ag NCs against MDR bacterial strains is summarized in Table 3.

3.4.3. Confocal laser scanning electron microscope

The uptake of Ag NPs and CS/Ag NCs binding into the intracellular of ESBL positive carbapenems resistant *P. aeruginosa* was visualized by CLSM. The result of Ag NPs and CS/Ag NCs treated *P. aeruginosa* cell show the complete and successful uptake of the nanomaterials by *P. aeruginosa* cell at their respective MIC. The uptake was more particularly high for CS/Ag NCs treated *P. aeruginosa* compared to Ag NPs. Maxima cell disruption of damaged cells of 100% and 72% were observed for CS/Ag NCs and Ag NPs at their respective MIC, respectively (Fig. 7a–c). After 24 h treatment at MIC, the attachment of both nanomaterials produced damages of surface integrity in *P. aeruginosa*. After their entry into the cell membrane, both nanomaterials collapsed the aggregation of cells and also showed crashed cell membrane with dispersed cell arrangement. The clear morphology with tightly packed aggregation of cells with intense adherent ability was, however, observed in untreated control cells. Acridine orange/Ethidium bromide are coloring dyes, which are used for detection of live cell death in nanomaterials treated or untreated bacteria. Here, the EtBr of treated cells indicate that negative charges of the *P. aeruginosa* cell membrane was easily affected by neutral charges of the Ag NPs, and the maximum uptake of nanomaterials was shown in treated *P. aeruginosa*. Due to this defect, the death cell rate gradually increased, and the colonies experienced

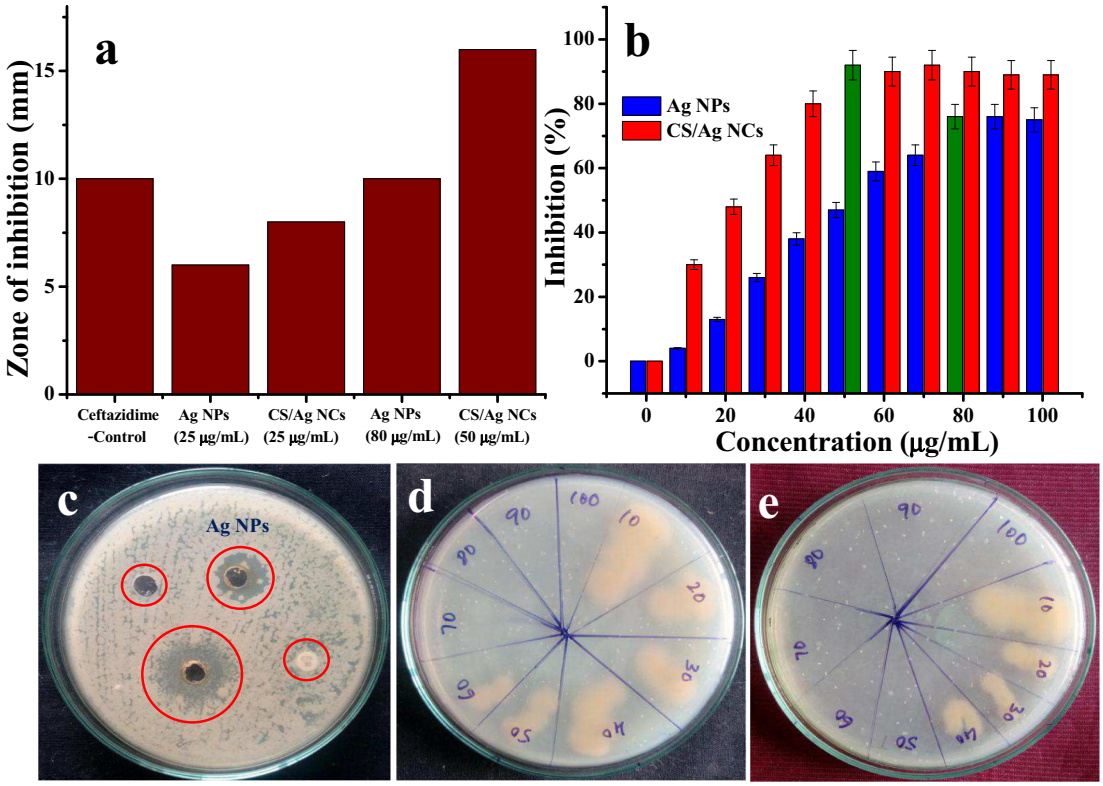

Fig. 6. Antibacterial activity of Ag NPs and CS/Ag NCs against ESBL positive *P. aeruginosa* BDU 5 (a), MIC of Ag NPs and CS/Ag NCs against ESBL positive *P. aeruginosa* BDU 5 (b). Agar well diffusion method differentiation of Ag NPs and CS/Ag NCs activity against *P. aeruginosa* BDU 5 (c), MBC of Ag NPs (d) and CS/Ag NCs (e) against ESBL positive *P. aeruginosa* BDU 5.

morphological damage as seen in red color images by uptake of EtBr. The untreated control cells of the *P. aeruginosa* cells, however, uptaked the AO stain, which showed smooth, clear membrane structure with green color morphology. Hence, the result demonstrated that the ESBL producing carbapenems resistant *P. aeruginosa* is highly sensitive to Ag NPs and CS/Ag NCs. A previous study reported that Ag NPs act as an effective antibiotic and altered the protein or metabolic pathway in MDR strains [78]. Our result agrees with another study where Ag^{+} ion from Ag NPs were shown to exert their activity against MDR bacterial strains with broad range of mechanism, including 30S ribosome sub unit, decreasing the expression of enzymes and protein essential to ATP production [79]. CLSM was used to detect the live, death cells of both nanomaterials treated, and untreated bacteria due to the uptake of AO/EB dye, coloring agents used to penetrate the damaged or smooth bacterial cells [80].

3.4.4. Scanning electron microscope

The morphological alteration of Ag NPs and CS/Ag NCs treated and untreated carbapenems resistant *P. aeruginosa* cell wall as well as its interior is shown in Fig. 7d,e. After treatment of the bacteria with both nanomaterials, the intracellular distribution and binding location of both nanomaterials as well as damaged morphology of bacteria was observed by using SEM. SEM images suggest that the treated cells possess a relatively rough surface, disorganized structure with distorted membrane morphology, large leakage of cellular content, irregular surface, collapsed membrane and bleb formation. The misshapen and fragmentary morphology of some cells with partially degraded intracellular damage was observed at the MIC of Ag NPs treated cells. The rod shaped, smooth, native cells and cleared filaments around the cells were, however, observed in the control images. The SEM results, however, revealed that CS/Ag NCs has a better ability to inhibit and intracellular modification in ESBL producing carbapenems resistant *P. aeruginosa* compared to Ag NPs. Recently, a study reported than many pis and gaps appeared in SEM micrographs and that membrane attack occurred in GNB, where it could penetrate inside the cell and finally act at various sites [81]. SEM images of CS/Ag NCs confirmed the cell wall or folic acid damage and altered metabolic pathways, including protein or DNA replication, which has been observed in MDR bacteria [82]. The SEM images of CS/Ag NCs treated bacterial cells show that big gaps appeared in the cell membrane, and that bacteria were almost disorganized or fragmented into several parts. Permeability of Ag NPs causes damage in bacteria due to the phosphorus and sulfur containing compounds such as DNA, regulating enzymes [83].

Table 3
Previous reports of MIC compared to Ag NPs and CS/Ag NCs obtained from the present study against MDR bacterial strains.

S. no	Material	ESBL producing bacteria	Antimicrobial activity	MIC	References
1	Ag NPs	*E. coli*, *Klebsiella* sp. and *Proteus sp.*	20 µg/mL	20 µg/mL	[72]
2	Ag NPs	*E. coli*	50 µg/mL	50 µg/mL	[73]
3	Ag NPs	*E. coli*	50 mmol/L	10.9–16.9 mmol/L	[74]
4	Ag NPs	KPC-positive *K. pneumoniae*	6.75 mg/mL	6.75 mg/mL	[75]
5	Ag NPs	*P. aeruginosa*	80 µg/mL	80 µg/mL	Present study
6	CS/Ag NCs	Methicillin-Resistant *S. aureus*	9.6 µg/mL	9.6 µg/mL	[76]
7	CS/Ag NCs	*S. aureus*, *P. aeruginosa* and methicillin resistant *S. aureus*	184.5 µg/mL	184.5 µg/mL	[77]
8	CS/Ag NCs	*P. aeruginosa*	40 µg/mL	40 µg/mL	Present study

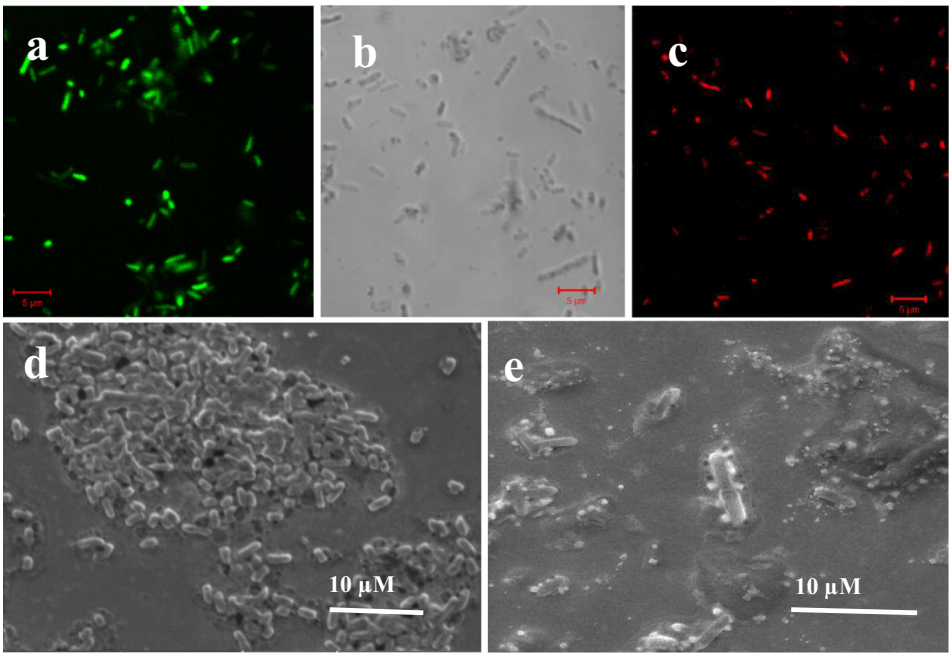

Fig. 7. CLSM images of Ag NPs and CS/Ag NCs against *P. aeruginosa* BDU 5, control (a), negative image (b) treated (c) and SEM images of Ag NPs and Ag/Cs NCs against *P. aeruginosa*, control (d) and treated (e).

3.5. Anti-β-lactamase activity by iodimetric assay

MIC of Ag NPs and CS/Ag NCs treated carbapenems resistant *P. aeruginosa* culture was observed in decolorization of dark blue color at 1 h incubation. The result indicated that the nanomaterial is involved in the β-lactam ring cleavage and induce β-lactamase inhibition activity in ESBL positive carbapenems resistant *P. aeruginosa* (Fig. 8a,b). The persistent blue color in the amoxicillin treated positive control indicate that

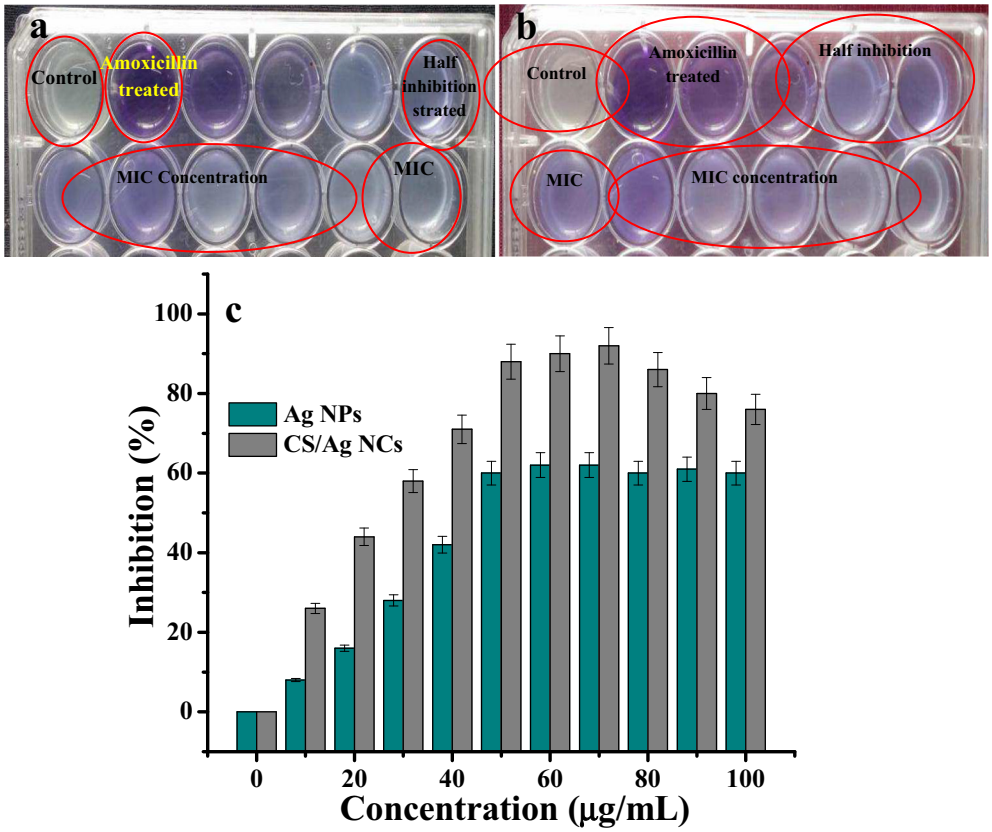

Fig. 8. Inhibition of β-lactamase by Ag NPs treated or control cells of the *P. aeruginosa* BDU 5 (24 well plate) plate (a), inhibition of β-lactamase by CS/Ag NCs treated or control cells of *P. aeruginosa* BDU 5 (24 well plate) plate was observed (b) and percentage of β-lactamase inhibition at various concentration using Ag NPs and CS/Ag NCs against *P. aeruginosa* BDU 5 (c).

the antibiotics did not undergo the β-lactam ring cleavage activity, which indicated that the ESBL production was not altered in *P. aeruginosa* culture. The result suggested that both nanomaterials had efficient β-lactamase inhibition activity. In the mechanism of β-lactamase inhibition, the oxidation process was initiated in Ag NPs and CS/Ag NCs treated samples due to the penicilloic acid degradation. Penicilloic acid is a punch of acids which formed from the penicillins by the hydrolytic opening of the lactam ring [39]. However, the free iodine easily binds to starch molecules of Ag NPs and CS/Ag NCs by degradation and produces blue color, indicating the nanomaterials possess β-lactamase inhibition activity. Furthermore, the anti-β-lactamase activity of Ag NPs and CS/Ag NCs treated bacterial culture was measured spectroscopically for detection of inhibition percentage. β-lactamase inhibition levels of 80% and 92% against ESBL positive carbapenems resistant *P. aeruginosa* were observed at concentrations of 70 and 50 μg/mL of nanomaterial, respectively. Before, the initiation of inhibition level in the Ag NPs and CS/Ag NCs against carbapenems resistant *P. aeruginosa* culture was observed at 10 and 5 μg/mL, respectively. This result allowed demonstrating that the Ag NPs and CS/Ag NCs have the ability to inhibit the β-lactamases production in ESBL positive *P. aeruginosa*. Furthermore, the β-lactamase inhibition percentages of the control and test samples were obtained by OD values using ELIZA reader and the result are shown in Fig. 8c. The outer membrane of proteins is the prime target for β-lactamase producing bacteria was found to contain large molecules of penicillin binding protein. Ag NPs and CS/Ag NCs may degrade the synthesis of penicillinase in ESBL producing bacteria due to the diffusion of nanomaterials through porins [84]. It is generally a reduction of the amount of these proteins, or some other components of the outer membrane, which causes the non-enzymatic mechanism of resistance. This may offer a chance to abolish the ESBL producing bacteria in urinary tract infected patients [1].

3.6. In-vivo toxicity analysis of Ag NPs and CS/Ag NCs

The toxicity study performed using adult *A. franciscana* allowed the determination of the lethal doses or minimum lethal concentrations (50%) of the Ag NPs and CS/Ag NCs treated animals (LD_{50} or LC_{50}), which was observed at 24 h. The mortality was reported based on the concentration of the nanomaterials, which showed minimum mortality at 10 μg/mL (3 nos) and maximum (22 nos) at 100 μg/mL of Ag NPs after 24 h. 8 no adult *Artemia* mortality were, however, recorded at 10 μg/mL concentration and 29 adult *Artemia* death was observed at 100 μg/mL concentration of CS/Ag NCs. Consequently, the optimum mortality of Ag NPs treated adult *Artemia* was 20 at concentrations of 70 and 80 μg/mL. Similar mortality rate was observed at concentrations of 40 and 60 μg/mL of CS/Ag NCs. The CS/Ag NCs concentration was comparatively very low compared to Ag NPs alone (Fig. 9a,b). The result revealed that the Ag NPs and CS/Ag NCs were highly toxicity against model marine organisms of *A. franciscana*, and that CS/Ag NCs possess stronger toxicity effect than Ag NPs alone. Furthermore, based on the minimum and maximum lethal concentration, the internal parts of the *A. franciscana* intestine was found to be heavily affected by CS/Ag NCs and the affected parts imaged by light microscopic analysis are shown in Fig. 9c–g. The internal parts of the partial damage of *A. franciscana* intestine was observed at 10 μg/mL treatment for both Ag NPs and CS/Ag NCs (Fig. 9d,f). The entire damage, however, was observed at a concentration of 100 μg/mL for both Ag NPs and CS/Ag NCs (Fig. 9e,g). The clear, unaffected control A. *franciscana* internal parts are reported in Fig. 9c.

4. Conclusion

In summary, Ag NPs and CS/Ag NCs were successfully synthesized by a simple chemical approach. The powder XRD patterns and TGA traces of Ag NPs and CS/Ag NCs suggested that highly pure Ag NPs and CS/Ag NCs were obtained. The TEM images of the CS/Ag NCs showed that Ag NPs form clusters that are surrounded by the CS matrix. CS/Ag NCs demonstrated excellent antibacterial activity against ESBL positive carbapenems resistant *P. aeruginosa* BDU 5 strain with a 20 mm ZOI at a concentration of 50 μg/mL, which was higher than for Ag NPs (16 mm at 80 μg/mL). MIC and MBC of CS/Ag NCs showed 92% of inhibition at concentrations of 50 μg/mL and 76% at 80 μg/mL, respectively. A syngergetic effects between Ag NPs and CS might explain why CS/Ag NCs exhibit greater antibacterial activity compared to when Ag NPs are used alone. CS controls the release of Ag + and promotes prolonged effect of Ag + as a function of time. CS macromolecules present in CS/Ag NCs may induce a positive charge to Ag NPs external side, which may increase their attaching to the negative charges of the bacterial cell surface. CLASM and SEM images allowed observing live death cell and intercellular damage of ESBL positive carbapenems resistant *P. aeruginosa* BDU 5 using CS/Ag NCs. The toxicity study of CS/Ag NCs against adult *A. franciscana* assay suggested that the material was highly toxic. Overall, CS/Ag NCs exhibited sufficient antibacterial and anti-ESBL

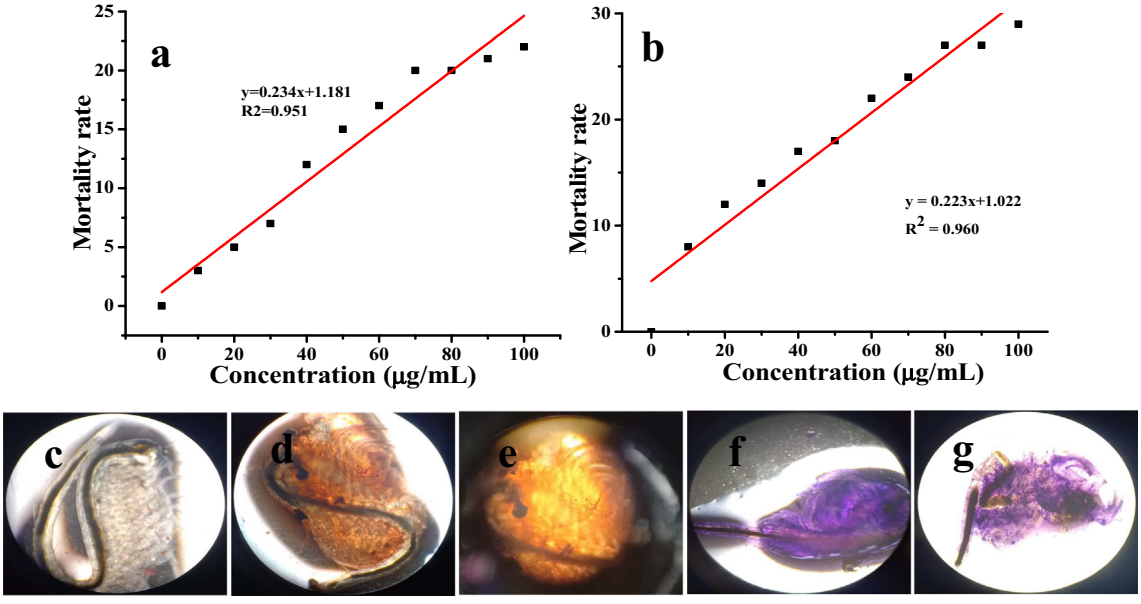

Fig. 9. Mortality rate of Ag NPs and CS/Ag NCs treated (a, b) against *A. franciscana*, internal damaged parts variation of *A. franciscana* intestine control (c), treatment at 10 μg/mL (d, f), and treatment at 100 μg/mL of Ag NPs and CS/Ag NCs (e, g), respectively.

properties against ESBL positive carbapenems resistant *P. aeruginosa* strain as well as toxicity against adult *A. franciscana* showing good potential to be used as antimicrobial agent in the biomedical sector.

Ethical consideration

The samples were approved by the ethics review committee (S·No of IEC Management office: DM/2016/101/55), Department of Microbiology, Bharathidasan University, Tiruchirappalli, Tamil Nadu, India. The permission was sought from the hospital and laboratory authorities. The ethical principles of scientific research as well as related national laws and regulations were adhered to.

Acknowledgement

M. M. and F. Q. acknowledge financial support from FONDECYT (Chile) under the Postdoctoral Fellowship No. 3180128. Acknowledgments are extended to the Department of Marine Science, Bharathidasan University, India for supporting toxicity analysis as well as the Department of Microbiology, K.A.P.V. Government Medical College & Hospital, Tiruchirappalli, Tamil Nadu, India for providing the bacterial culture isolated from urinary tract infection patients.

Conflict of interest

The authors declare no conflict of interest.

References

[1] C.H.N. Barros, S. Fulaz, D. Stanisic, L. Tasic, Nanosilver against multidrug-resistant bacteria (MDRB), Antibiotics 69 (2018) 1–24.
[2] G. Rajivgandhi, M. Maruthupandy, G. Ramachandran, M. Priyanga, N. Manoharan, Detection of ESBL genes from ciprofloxacin resistant Gram-negative bacteria isolated from urinary tract infections (UTIs), Front. Lab. Med. 2 (2018) 5–13.
[3] A. Gupta, N.M. Saleh, R. Das, R.F. Landis, A. Bigdeli, K. Motamedchaboki, A. Rosa Campos, Kenneth Pomeroy, Morteza Mahmoudi, Vincent M. Rotello, Synergistic antimicrobial therapy using nanoparticles and antibiotics for the treatment of multidrug-resistant bacterial infection, Nano Futures 1 (2017), 015004.
[4] G. Rajivgandhi, G. Ramachandran, M. Maruthupandy, B. Vaseeharanc, N. Manoharan, Molecular identification and structural characterization of marine endophytic actinomycetes Nocardiopsis sp. GRG 2 (KT 235641) and its antibacterial efficacy against isolated ESBL producing bacteria, Microb. Pathog. 126 (2019) 138–148.
[5] M. Exner, S. Bhattacharya, B. Christiansen, J. Gebel, P. Goroncy-Bermes, P. Hartemann, Antibiotic resistance: what is so special about multidrug-resistant gram-negative bacteria? GMS Hyg. Inf. Cont. 12 (2017) 1–24.
[6] K. Nepal, N.D. Pant, B. Neupane, A. Belbase, R. Baidhya, R.K. Shrestha, Extended spectrum beta-lactamase and metallo beta-lactamase production among Escherichia coli and *Klebsiella pneumoniae* isolated from different clinical samples in a tertiary care hospital in Kathmandu, Ann. Clin. Microbiol. Antimicrob. 16 (2017) 62.
[7] P. Kumar, A. Kaushik, E.P. Lloyd, S.G. Li, R. Mattoo, N.C. Ammerman, D.T. Bell, A.L. Perryman, T.A. Zandi, S. Ekins, S.L. Ginell, C.A. Townsend, J.S. Freundlich, G. Lamichhane, Non-classical transpeptidases yield insight into new antibacterials, Nat. Chem. Biol. 13 (2017) 54–61.
[8] Z. Lifshitz, N. Sturlesi, M. Parizade, S.F. Blum, M. Gordon, D. Taran, Distinctiveness and similarities between extended-spectrum β-lactamase-producing *Escherichia coli* isolated from cattle and the community in Israel, Microb. Drug Resist. 24 (2018) 868–875.
[9] J.K. Johnson, G.L. Robinson, L.L. Pineles, A.O. Ajao, L. Zhao, J.S. Albrecht, A.D. Harris, K.A. Thom, J.P. Furuno, Carbapenem MICs in *Escherichia coli* and *Klebsiella* species producing extended-spectrum β-lactamases in critical care patients from 2001 to 2009, Antimicrob. Agent. Chemothe. 61 (2017) (e01718-16).
[10] G. Rajivgandhi, R. Vijayan, M. Maruthupandy, B. Vaseeharan, N. Manoharan, Antibiofilm effect of *Nocardiopsis* sp. GRG 1 (KT235640) compound against biofilm forming Gram negative bacteria on UTIs, Microb. Pathog. 118 (2018) 190–198.
[11] S. Shaikh, J. Fatima, S. Shakil, S.M. Rizvi, M.A. Kamal, Antibiotic resistance and extended spectrum beta-lactamases: types, epidemiology and treatment, Saudi J. Biolog. Sci. 22 (2015) 90–101.
[12] WHO, Global priority list of antibiotic-resistant bacteria to guide research, discovery, and development of new antibiotics, http://www.who.int/medicines/publications/global-priority-list-antibiotic-resistant-bacteria/en/ 1–7 (2017).
[13] G. Raman, E.E. Avendano, J. Chan, S. Merchant, L. Puzniak, Risk factors for hospitalized patients with resistant or multidrug-resistant *Pseudomonas aeruginosa* infections: a systematic review and meta-analysis, Antimicrob. Resis. Inf. Con. 7 (2018) 7–9.
[14] A. Liakopoulos, J. Betts, R. La Ragione, A. van Essen-Zandbergen, D. Ceccarelli, E. Petinaki, Occurrence and characterization of extended-spectrum cephalosporin-resistant Enterobacteriaceae in healthy household dogs in Greece, J. Med. Microb 67 (2018) 931–935.
[15] M.D. Obritsch, D.N. Fish, R. MacLaren, R. Jung, National surveillance of antimicrobial resistance in *Pseudomonas aeruginosa* isolates obtained from intensive care unit patients from 1993 to 2002, Antimicrob, Agent. Chemother. 48 (2014) 4606–4610.
[16] S. Mukherjee, C.R. Patra, Biologically synthesized metal nanoparticles: recent advancement and future perspectives in cancer theranostics, Future Science OA 3 (9) (2017), FSO203. https://doi.org/10.4155/fsoa-2017-0035.
[17] P. Kuppusamy, M.M. Yusoff, G.P. Maniam, Govindan, Biosynthesis of metallic nanoparticles using plant derivatives and their new avenues in pharmacological applications – an updated report, Saudi Pharm. 24 (2016) 473–484.
[18] X.F. Zhang, Z.G. Liu, W. Shen, S. Gurunathan, Silver nanoparticles: synthesis, characterization, properties, applications, and therapeutic approaches, Int. J. Mol. Sci. 17 (2016) 1534, https://doi.org/10.3390/ijms17091534.
[19] G. Rajivgandhi, M. Maruthupandy, T. Muneeswaran, M. Anand, N. Manoharan, Antibiofilm activity of zinc oxide nanosheets (ZnO NSs) using *Nocardiopsis* sp. GRG1 (KT235640) against MDR strains of gram negative *Proteus mirabilis* and *Escherichia coli*, Process Biochem. 67 (2018) 8–18.
[20] M. Maruthupandy, G. Rajivgandhi, T. Muneeswaran, J.-M. Song, N. Manoharan, Biologically synthesized zinc oxide nanoparticles as nanoantibiotics against ESBLs producing gram negative bacteria, Microb. Pathog. 121 (2018) 224–231.
[21] I. Khan, K. Saeed, I. Khan, Nanoparticles: properties, applications and toxicities, Arab. J. Chem. (2017)https://doi.org/10.1016/j.arabjc.2017.05.011 (In Press).
[22] Z. Zhong, S. Luo, K. Yang, X. Wu, T. Ren, High-performance anionic waterborne polyurethane/Ag nanocomposites with excellent antibacterial property via in situ synthesis of Ag nanoparticles, RSC Adv. 7 (2017), 42296.
[23] M.W. Tibbitt, C.B. Rodell, J.A. Burdick, K.S. Anseth, Progress in material design for biomedical applications, Proceed. Nation. Acad. Sci. U.S.A 112 (2015) 14444–14451.
[24] M. Biondi, A. Borzacchiello, L. Mayol, L. Ambrosio, Nanoparticle-integrated hydrogels as multifunctional composite materials for biomedical applications, Gels 1 (2015) 162–178.
[25] X. Wang, Z. Wang, J. Zhang, H.X. Qi, J. Chen, M. Xu, Cytotoxicity of AgNPs/CS composite films: AgNPs immobilized in chitosan matrix contributes a higher inhibition rate to cell proliferation, Bioeng 7 (2016) 283–290.
[26] X. Huang, X. Bao, Z. Wang, Q. Hu, A novel silver-loaded chitosan composite sponge with sustained silver release as a long-lasting antimicrobial dressing, RSC Adv. 7 (2017) 34655–34663.
[27] B.V. Bonifácio, P.B. da Silva, M.A. dos Santos Ramos, K.M. Silveira Negri, T.M. Bauab, M. Chorilli, Nanotechnology-based drug delivery systems and herbal medicines: a review, Int. J. Nanomedicine 9 (2014) 1–15.
[28] C. Nunes, M.A. Coimbra, P. Ferreira, Tailoring functional chitosan-based composites for food applications, Chem. Rec. 18 (2018) 1138–1149.
[29] Z. Wu, X. Huang, Y.-C. Li, H. Xiao, X. Wang, Novel chitosan films with laponite immobilized Ag nanoparticles for active food packaging, Carbohyd. Polym. 199 (2018) 210–218.
[30] M. Maruthupandy, G. Rajivgandhi, T. Muneeswaran, T. Vennila, F. Quero, J.M. Song, Chitosan/silver nanocomposites for colorimetric detection of glucose molecule, Int. Biolog. Macromol. 121 (2019) 822–828.
[31] M.T. Akhi, R. Ghotaslou, N. Alizadeh, T. Pirzadeh, S. Beheshtirouy, M. Yousef Mema, High frequency of MRSA in surgical site infections and elevated vancomycin MIC, Wound Medicine 17 (2017) 7–10.
[32] C. Navarro-San Francisco, M. Mora-Rillo, M.P. Romero-Gómez, F. Moreno-Ramos, A. Rico-Nieto, G. Ruiz-Carrascoso, Bacteraemia due to OXA-48-carbapenemase-producing Enterobacteriaceae: a major clinical challenge, Clin. Microbiol. Inf. 19 (2013) 72–79.
[33] M.P. Mishra, R.N. Padhy, Antibacterial activity of green silver nanoparticles synthesized from *Anogeissus acuminata* against multidrug resistant urinary tract infecting bacteria *in vitro* and host-toxicity testing, J. Appl. Biomed. 16 (2018) 120–125.
[34] N.A. Al-Dhabi, A.M. Ghilan, M.V. Arasu, V. Duraipandiyan, Green biosynthesis of silver nanoparticles produced from marine Streptomyces sp. Al-Dhabi-89 and their potential applications against wound infection and drug resistant clinical pathogens, J. Photochem. Photobiol. B 189 (2018) 176–184.
[35] Y.H. Liu, S.C. Kuo, B.Y. Yao, Z.S. Fang, Y.T. Lee, Y.C. Chang, Colistin nanoparticle assembly by coacervate complexation with polyanionic peptides for treating drug-resistant gram-negative bacteria, Acta Biomater. 82 (2018) 133–142.
[36] N. Yadav, A. Dubey, S. Shukla, C.P. Saini, G. Gupta, R. Priyadarshini, Graphene oxide-coated surface: inhibition of bacterial biofilm formation due to specific surface-interface interactions, ACS Omega 2 (2017) 3070–3082.
[37] A.M. Bardbari, M.R. Arabestani, M. Karami, F. Keramat, H. Aghazadeh, M.Y. Alikhani, Highly synergistic activity of melittin with imipenem and colistin in biofilm inhibition against multidrug-resistant strong biofilm producer strains of *Acinetobacter baumannii*, Europ. J. Clin. Microbiol. Infect. Dis. 37 (2018) 443–454.
[38] S. Arora, S. Paul Nandi, Reversion of antibiotic resistance with beta-lactamase inhibitor from medicinal plants, Asian J. Pharm. Clin. Res. 10 (9) (2017) 1–5.
[39] B.N. Meyer, N.R. Ferrigni, J.E. Putnam, L.B. Jacobsen, D.E. Nichols, J.L. McLaughlin, Brine shrimp: a convenient general bioassay for active plant constituents, Planta Med. 45 (1982) 31–34.
[40] G. Van Stappen, Introduction, biology and ecology of Artemia, Manual on the Production and Use of Live Food for Aquaculture, vol. 361, 1996, pp. 79–106.
[41] S. Peng, J.M. McMahon, G.C. Schatz, S.K. Gray, Y. Suna, Reversing the size-dependence of surface plasmon resonances, Proc. Natl. Acad. Sci. U. S. A. 107 (2010) 14530–14534.
[42] S. Iravani, H. Korbekandi, S.V. Mirmohammadi, B. Zolfaghari, Synthesis of silver nanoparticles: chemical, physical and biological methods, Res. Pharma. Sc. 9 (2014) 385–406.

[43] B. Khodashenas, H.R. Ghorbani, Synthesis of silver nanoparticles with different shapes, Arab. J. Chem. (2015)https://doi.org/10.1016/j.arabjc.2014.12.014 (In Press).
[44] K. Shameli, M.B. Ahmad, M. Zargar, W. Md Zin, W. Yunus, N.A. Ibrahim, Synthesis and characterization of silver/montmorillonite/chitosan bionanocomposites by chemical reduction method and their antibacterial activity, Int. J. Nanomedicine 6 (2011) 271–284.
[45] S. Govindan, E.A.K. Nivethaa, R. Saravanan, V. Narayanan, A. Stephen, Synthesis and characterization of chitosan–silver nanocomposite, Appl. Nanosci. 2 (2012) 299–303.
[46] S. Jena, R.K. Singh, B. Panigrahi, D. Suar, D. Mandal, Photo-bioreduction of Ag+ ions towards the generation of multifunctional silver nanoparticles: mechanistic perspective and therapeutic potential, J. Photochem. Photobiol. B: Biology 164 (2016) 306–313.
[47] A.P. Martinez-Camacho, M.O. Cortez-Rocha, J.M. Ezquerra-Brauer, A.Z. Graciano Verdugo, F. Rodriguez-Felix, M.M. Castillo-Ortega, Chitosan composite film: thermal, structural, mechanical and antifungal properties, Carbohyd. Polym. 82 (9) (2010) 305–515.
[48] E. Susilowati, I. Kartini, S.J. Santosa, A. Triyono, Effect of glycerol on mechanical and physical properties of silver-chitosan nanocomposite films, IOP Conf. Series: Mat. Sci. Eng. 107 (9) (2016) 012041, https://doi.org/10.1088/1757-899X/107/1/012041.
[49] V.K. Rana, A.K. Pandey, R.P. Singh, Enhancement of thermal stability and phase relaxation behavior of chitosan dissolved in aqueous l-lactic acid: using 'silver nanoparticles' as nano filler, Macromol. Res. 18 (2010) 713–720.
[50] M. Raffi, F. Hussain, T.M. Bhatti, J.I. Akhter, A. Hameed, M.M. Hasan, Antibacterial characterization of silver nanoparticles against *E. coli* ATCC-15224, J. Mat. Sci. Technol. 24 (2008) 192–196.
[51] K. Yoshizuka, Z. Lou, K. Inoue, Silver-complexed chitosan microparticles for pesticide removal, React. Funct. Polym. 44 (2000) 47–54.
[52] G. Rajivgandhi, M. Maruthupandy, N. Manoharan, Detection of TEM and CTX-M genes from ciprofloxacin resistant *Proteus mirabilis* and *Escherichia coli* isolated on urinary tract infections (UTIs), Microb. Pathog. 121 (2018) 123–130.
[53] E.S. Yılmaz, N.C. Guvensen, In vitro biofilm formation in ESBL producing *Escherichia coli* isolates from cage birds, Asian Pacif. J. Trop. Med. 9 (2016) 1069–1074.
[54] G. Rajivgandhi, T. Muneeswaran, M. Maruthupandy, C.M. Ramakritinan, K. Saravanan, V. Ravikumar, Antibacterial and anticancer potential of marine endophytic actinomycetes *Streptomyces coeruleorubidus* GRG 4 (KY457708) compound against colistin resistant uropathogens and A549 lung cancer cells, Microb. Pathog. 125 (2018) 325–335.
[55] A. Mazzariol, A. Bazaj, G. Cornaglia, Multi-drug-resistant Gram-negative bacteria causing urinary tract infections: a review, J. Chemothe. 29 (2017) 2–9.
[56] K. Ramakrishnan, S. Rajagopalan, S. Nair, P. Kenchappa, S.D. Chandrakesan, Molecular characterization of metallo β-lactamase producing multidrug resistant *Pseudomonas aeruginosa* from various clinical samples, Indian J. Patholog. Microbiol. 57 (2014) 579–582.
[57] E. Vedel, Simple method to determine b-lactam resistance phenotypes in *Pseudomonas aeruginosa* using the disc agar diffusion test, J. Antimicrob. Chemothe. 56 (2005) 657–664.
[58] D.M. Zerr, S.J. Weissman, C. Zhou, M.P. Kronman, A.L. Adler, J.E. Berry, The molecular and clinical epidemiology of extended-spectrum cephalosporin- and carbapenem-resistant enterobacteriaceae at 4 US pediatric hospitals, J. Ped. Infect. Diseas. Societ. 6 (2007) 366–375.
[59] P. Cheddie, F. Dziva, P.E. Akpaka, Detection of a CTX-M group 2 beta-lactamase gene in a *Klebsiella pneumoniae* isolate from a tertiary care hospital, Trinidad and Tobago, Annal. Clin. Microbiol. Antimicrob. 16 (2017), 33. https://doi.org/10.1186/s12941-017-0209-x.
[60] A. Poulou, E. Grivakou, G. Vrioni, V. Koumaki, T. Pittaras, S. Pournaras, Modified CLSI extended-spectrum β-lactamase (ESBL) confirmatory test for phenotypic detection of ESBLs among Enterobacteriaceae producing various β-lactamases, J. Clin. Microb. 52 (2014) 1483–1489.
[61] X. Zhang, F. Yang, J. Zou, W. Wu, H. Jing, Q. Gou, Immunization with *Pseudomonas aeruginosa* outer membrane vesicles stimulates protective immunity in mice, Vaccine 36 (2018) 1047–1054.
[62] G. Wijesinghe, A. Dilhari, B. Gayani, N. Kottegoda, L.P. Samaranayake, M. Weerasekera, Influence of laboratory culture media on in-vitro growth, adhesion and biofilm formation of *Pseudomonas aeruginosa* and *Staphylococcus aureus*, Med. Princ. Pract. (2018)https://doi.org/10.1159/000494757.
[63] M.A. Elgadir, M.S. Uddin, S. Ferdosh, A. Adam, A.J.K. Chowdhury, M.Z.I. Sarker, Impact of chitosan composites and chitosan nanoparticle composites on various drug delivery systems: a review, J. Food Drug Anal. 23 (2015) 619–629.
[64] Z. Shen, G. Han, X. Wang, J. Luo, R. Suna, An ultra-light antibacterial bagasse–AgNP aerogel, J. Mater. Chem. B 5 (2017) 1155.
[65] L. Wang, C. Hu, C. Shao, The antimicrobial activity of nanoparticles: present situation and prospects for the future, Int. J. Nanomedicine 12 (2017) 1227–1249.
[66] P.V. Baptista, M.P. McCusker, A. Carvalho, D.A. Ferreira, N.M. Mohan, M. Martins, Nano-strategies to fight multidrug resistant bacteria—a battle of the titans, Front. Microbiol. 9 (2018) 1441, https://doi.org/10.3389/fmicb.2018.01441.
[67] A. Regiel-Futyra, L. Li skiewicz, V. Sebastian, M. Irusta, A. Arruebo, G. Kyzioła, Development of noncytotoxic silver–chitosan nanocomposites for efficient control of biofilm forming microbes, RSC Adv. 7 (52398) (2017) 1–16.
[68] L.O. Cinteza, C. Scomoroscenco, S.N. Voicu, C.L. Nistor, S.G. Nitu, B. Trica, Chitosan-stabilized Ag nanoparticles with superior biocompatibility and their synergistic antibacterial effect in mixtures with essential oils, Nanomat. (Basel) 8 (2018), E826.
[69] M. Jose, A.A. Cesar, Mechanisms of antibiotic resistance, Microbiol. Spectr. 4 (2016) (0016-2015).
[70] J. Terry Beveridge, Structures of gram-negative cell walls and their derived membrane vesicles, J. Bacteriol. 181 (1999) 4725–4733.
[71] G. Matthieu, N. Gagnon Raktim, B. Roy Ivan, S. Lomakin Tanja Florin Alexander, A. Mankin Thomas, Steitz, Structures of proline-rich peptides bound to the ribosome reveal a common mechanism of protein synthesis inhibition, Nucleic Acids Res. 44 (2016) 2439–2450.
[72] A. Banu, V. Rathod, E. Ranganath, Silver nanoparticle production by *Rhizopus stolonifer* and its antibacterial activity against extended spectrum b-lactamase producing (ESBL) strains of Enterobacteriaceae, Mat. Res. Bull. 46 (2011) 1417–1423.
[73] D. Manikprabhu, K. Lingappa, Synthesis of silver nanoparticles using the *Streptomyces coelicolorklmp* 33 pigment: an antimicrobial agent against extended-spectrum beta-lactamase (ESBL) producing *Escherichia coli*, Mater. Sci. Eng. C Mater. Biol. Appl. 45 (2014) 434–437.
[74] D. Kar, S. Bandyopadhyay, U. Dimri, D. Brata Mondal, P. Nanda, A. Das, Antibacterial effect of silver nanoparticles and capsaicin against MDR-ESBL producing *Escherichia coli*: an in vitro study, Asian. Pac. J. Trop. Dis. 6 (2016) 807–810.
[75] A. Panacek, M. Smekalov, R. Vecerov, K. Bogdanov, M. Roderov, Kolar, Silver nanoparticles strongly enhance and restore bactericidal activity of inactive antibiotics against multi resistant Enterobacteriaceae, Collo. Surf. B Biointerf. 142 (2016) 392–399.
[76] V. Holubnych, O. Kalinkevich, O. Ivashchenko, M. Pogorielov, Antibacterial activity of in situ prepared chitosan/silver nanoparticles solution against methicillin-resistant strains of *Staphylococcus aureus*, Nanos. Res. Lett. 13 (2018) 71, https://doi.org/10.1186/s11671-018-2482-9.
[77] A. Shah, I. Hussain, G. Murtaza, Chemical synthesis and characterization of chitosan/silver nanocomposites films and their potential antibacterial activity, Int. J. Biol. Macromol. 116 (2018) 520–529.
[78] H.H. Lara, L.V. Ayala-Nunez, L. Carmen, I. Turrent, C.R. Padilla, Bactericidal effect of silver nanoparticles against multidrug-resistant bacteria, World J. Microbiol. Biotech. 26 (2010) 615–621.
[79] B. Das, S.K. Dash, D.T. Mandal, S. Chattopadhyay, S. Tripathy, Green synthesized silver nanoparticles destroy multidrug resistant bacteria via reactive oxygen species mediated membrane damage, Arab. J. Chem. 10 (2017) 862–876.
[80] M.A. Ansari, H.M. Khan, A.A. Khan, S.S. Cameotra, S. Pal, Antibiofilm efficacy of silver nanoparticles against biofilm of extended spectrum b-lactamase isolates of *Escherichia coli* and *Klebsiella pneumonia*, Appl. Nanosci. 4 (2014) 859–868.
[81] A. Pompilio, C. Geminiani, D. Bosco, R. Rana, A. Aceto, T. Bucciarelli, Electrochemically synthesized silver nanoparticles are active against planktonic and biofilm cells of *Pseudomonas aeruginosa* and other cystic fibrosis-associated bacterial pathogens, Front. Microbiol. 9 (2018), 1349. https://doi.org/10.3389/fmicb.2018.01349.
[82] A.J. Kora, R.B. Sashidhar, Biogenic silver nanoparticles synthesized with rhamnogalacturonan gum: antibacterial activity, cytotoxicity and its mode of action, Arab. J. Chem. 11 (2018) 313–323.
[83] A.S.A. El-Sayed, D. Ali, Biosynthesis and comparative bactericidal activity of silver nanoparticles synthesized by *Aspergillus flavus* and *Penicillium crustosum* against the multidrug-resistant bacteria, J. Microbiol. Biotechnol. (2018)https://doi.org/10.4014/jmb.1806.05089 (Accepted manuscript).
[84] J. Subashini, V. Gopiesh Khanna, K. Kannabiran, Anti-ESBL activity of silver nanoparticles biosynthesized using soil *Streptomyces* species, Biopro. Biosyst. Engin. 37 (2014) 999–1006.